Energy Conversion and Management 257 (2022) 115410

Contents lists available at ScienceDirect

Energy Conversion and Management

journal homepage: www.elsevier.com/locate/enconman

Thermodynamic and environmental analyses of a novel closed loop regasification system integrating ORC and CO_2 capture in floating storage regasification units

Manuel Naveiro [a,*], Manuel Romero Gómez [b], Ignacio Arias-Fernández [b], Álvaro Baaliña Insua [b]

[a] Energy Engineering Research Group, University Institute of Maritime Studies, ETSNM, University of A Coruña, Paseo de Ronda 51, A Coruña 15011, Spain
[b] Energy Engineering Research Group, University Institute of Maritime Studies, Nautical Sciences and Marine Engineering Department, ETSNM, University of A Coruña, Paseo de Ronda 51, A Coruña 15011, Spain

ARTICLE INFO

Keywords:
Floating storage regasification unit
Exergy analysis
Liquefied natural gas cold energy
Post-combustion CO_2 capture
Organic Rankine cycle

ABSTRACT

Regasification systems in Floating Storage Regasification Units (FSRUs) that use the steam generated by the boilers as the heat source (closed loop) in the liquefied natural gas (LNG) regasification process are less detrimental to the marine environment than those systems that use seawater (open loop). Their drawback, however, lies in the significant increase in fuel consumption and, thus, CO_2 emissions. The present paper performs an energy, exergy and environmental analysis of a novel closed-loop regasification system for FSRUs that integrates an organic Rankine cycle (ORC) and post-combustion CO_2 capture system with a 30 wt% aqueous solution of monoethanolamine (MEA). LNG cold energy is utilised for power generation through the ORC as well as in the processes of CO_2 capture, compression, drying and liquefaction. The system proposed is able to meet the electrical power demand of the FSRU without the use of dual fuel engines, while CO_2 capture efficiency in the boiler flue gases exceeds 90%. Fuel consumption is cut by 18% in this system in comparison with existing closed-loop regasification systems, and exergy efficiency increases by 14%, while CO_2 emissions decrease by approximately 75% compared to open-loop systems commonly installed on board.

1. Introduction

The Covid-19 pandemic drove down CO_2 emission levels by 5.02% in 2020 compared with the previous year [1]. In the year 2021, emissions will rebound two thirds of such decline and, unless appropriate measures are taken, emission levels for the year 2050 will be similar in value to the present [2].

In the maritime sector, transport-related global anthropogenic emissions accounted for 2.89% in 2018, implying a 4.71% rise in comparison with 2012 [3]. Since the first set of mandatory measures to cut ship emissions were adopted in 2011, the International Maritime Organization (IMO), aware of the urgent situation, aims to rapidly reduce greenhouse gas emissions by at least 50% from the 2008 level by 2050. To achieve such a goal, an initial strategy has been established with a series of possible measures for the short-term (between 2018 and 2023), medium-term (between 2023 and 2030) and long-term (beyond 2030) [4]. June 2021 saw the implementation of the first two short-term measures: The Energy Efficiency Existing Ship Index (EEXI) and the annual operational carbon intensity indicator (CII) [5]. However, the IMO's reduction target requires the uptake of low or zero-carbon fuel technologies which are currently yet to be fully developed [6]. Hence, the application of carbon capture and storage (CCS) technologies, such as those used in thermal plants and industrial processes, is a measure of particular interest to reduce CO_2 emissions from ships [7]. Conscious of this situation, well-known manufacturers of exhaust gas treatment systems in the marine industry such as Alfa Laval, Mitsubishi and Wärtsilä are participating in projects for the development of CCS systems on board vessels [8–10]. The CC-Ocean project, which employs a technique widely-known on shore of post-combustion capture with chemical absorption [11], has recently been the first to install a pilot CCS system on board a coal carrier [12].

Despite the interest in the application of CCS technologies in the shipping industry, on board CO_2 capture is scarcely covered in scientific literature. Luo et al. [13] simulate a capture system with a 35 wt% aqueous solution of monoethanolamine (MEA) to treat exhaust gases

* Corresponding author.
E-mail addresses: manuel.naveiro@udc.es (M. Naveiro), m.romero.gomez@udc.es (M. Romero Gómez), ignacio.arias@udc.es (I. Arias-Fernández), alvaro.baalina@udc.es (Á. Baaliña Insua).

https://doi.org/10.1016/j.enconman.2022.115410
Received 27 December 2021; Received in revised form 1 February 2022; Accepted 20 February 2022
Available online 26 February 2022

Nomenclature

Symbols

b	specific energy consumption (kJ/kg)
C_F	carbon factor (–)
e	specific flow exergy (kJ/kg)
$\dot{E}$	exergy flow rate (kW)
g	specific Gibbs energy (kJ/kg)
h	specific enthalpy (kJ/kg)
$\dot{H}$	energy flow rate (kW)
$\dot{I}$	irreversibilities (kW)
$\dot{m}$	mass flow rate (kg/s)
M	molar mass (kg/kmol)
n	moles (–)
p	pressure (bar)
$\dot{Q}$	heat transfer rate (kW)
s	specific entropy (kJ/kg-K)
T	temperature (°C)
v	specific volume (m^3/kg)
V	volume (m^3)
$\dot{W}$	power (kW)
y	mole fraction (–)
η	efficiency (–)
ρ	density (kg/m^3)
φ	chemical exergy factor for fuels (kJ/kg)

Subscripts and Superscripts

0	reference condition
AE	auxiliary engines
alt	alternator
b	base or boiler
ch	chemical
comb	combustion
comp	compressor
cond	condensables
el	electrical
ex	exergy
f	fuel
g	gases or group
i	inlet
l	liquid
LHV	lower heating value
m	mechanical, mixture or mixing
n	natural
non-cond	non-condensables
o	output
p	pressure or products
ph	physical
r	reactants
RB	regasification boilers
th	thermal
tk	storage tank
tot	total
turb	turbine

Abbreviations

ABS	absorber
AC/NGH	after cooler/natural gas heater
ADS	adsorber
BOG	boil off gas
BOR	boil off rate
C	compressor
CC	carbon capture
CCS	carbon capture and storage
CFRI	Carbon Footprint Regasification Indicator
CII	Carbon Intensity Indicator
DC	drain cooler/condenser
DF	dual fuel
DFDE	dual fuel diesel electric
DIPA	diisopropylamine
DSH	desuperheater
EEDI	Energy Efficiency Design Index
EERI	Energy Efficiency Regasification Indicator
EEXI	Energy Efficiency Existing Ship Index
FDF	forced draught fan
FGB	flue gas blower
FSRU	floating storage regasification unit
FT	feed tank
FV	forcing vaporizer
GCU	gas combustion unit
GCU-OL	seawater regasification system without recondenser
GWP	global warming potential
HFO	heavy fuel oil
IMO	International Maritime Organization
L/G	liquid/gas ratio (kg/kg)
LCO_2	liquefied CO_2
LCO2	CO_2 liquefier
LD	low duty
LNG	liquefied natural gas
MDEA	methyldiethanolamine
MEA	monoethanolamine
MX	mixer
NG	natural gas
ORC	organic Rankine cycle
ORC-OL	open loop propane regasification system with ORC
P	pump
PH	preheater
P-OL	open loop propane regasification system
PVP	propane vaporizer
PZ	piperazine
R	recondenser
REB	reboiler
RMH	rich mixture heater
S	separator
STR	stripper
SW-OL	seawater regasification system
T	steam trap or turbine
V	valve
VP	LNG vaporizer
WGC	water-glycol cooler
WG-CL	closed loop propane regasification system
WGH	water-glycol heater

from the propulsion system of a general cargo vessel with two internal combustion engines. The CCS system with the original propulsion achieves a capture efficiency of 73%, yet a value of 90% can be attained if a gas turbine is additionally installed, increasing fuel consumption by 21.41%. Feenstra et al. [14] carried out a techno-economic study of the CCS system with 30 wt% aqueous solutions of MEA and piperazine (PZ) for diesel or liquefied natural gas (LNG) fuelled vessels. The system proposed for LNG-fuelled vessels exploits the cooling capacity of the fuel vaporization process to liquefy the captured CO_2, while a refrigeration cycle with ammonia is employed in diesel-fuelled vessels. The results

obtained for capture efficiencies of 60% and 90% suggest that the CCS system with the PZ aqueous solution is more cost-efficient. Lee et al. [15] propose a new method in order to determine the Energy Efficiency Design Index (EEDI) of vessels, introducing a CO_2 emission reduction factor associated with the CCS system. This new methodology is applied to a container ship powered by a two-stroke dual fuel (DF) engine that has a PZ-activated methyldiethanolamine (MDEA) CCS system. With regard to the CO_2 liquefaction process, LNG cold energy is used through an intermediate fluid in the condenser of the refrigeration cycle with ammonia. Stec et al. [16] evaluate the EEDI decrease in a Handymax tanker with heavy fuel oil (HFO) as fuel, using a CCS system with a 30 wt % aqueous solution of MEA. The proposed system that exploits waste heat from the flue gases can easily fulfil the most demanding EEDI required level. Long et al. [17] developed a CO_2 capture system for a diesel engine similar to that of Feenstra et al. [14] and investigate ways of improving CO_2 capture in the absorber by means of solvents (MEA/PZ and MDEA/PZ), an intercooler and multifeed. The configuration with MDEA/PZ, implementing also the mentioned modifications in the absorber, improves capture efficiency by 8.4% in comparison with the base case. Ji et al. [18] study the impact of solvents, type of packing and the L/G ratio in a CCS system applied to an LNG vessel with four-stroke DF engines. Diisopropanolamine (DIPA) and MDEA/PZ solvents respectively obtain better results than the solution with MEA in terms of energy required for solvent regeneration and CO_2 emission reduction. Lastly, Güler and Ergin [19] investigate the effects of the hydraulic design parameters of the separation columns of the CCS system with a 35 wt% aqueous solution of MEA and carry out an economic assessment for a very large crude carrier (VLCC) and three types of LNG vessels (Q-Max, Q-Flex and conventional). The CCS system is compared to other CO_2 emission control methods, such as speed reduction and the use of LNG. The results obtained suggest that speed reduction is the cheapest and simplest alternative in the oil tanker (low freight cost), while the CCS system is more advantageous in large LNG vessels (high freight cost).

Most of the works published to date study the reduction of CO_2 emissions and the economic impact of CCS systems in two and four-stroke engines with different solvents, with the usual reference aqueous solution containing 30–35 wt% MEA. None of the studies, however, assess the CCS system from an exergy standpoint. Moreover, although literature exists on exploiting the energy from the vaporization process of LNG used as fuel (LNG-fuelled vessels) to liquefy CO_2, such amount of cold energy is negligible compared to that available in the Floating Storage Regasification Unit (FSRU) regasification process. The latter represents a major advantage for this type of vessel. To date, no research work associates regasification cold energy with CO_2 capture; all works are focused on the use of cold energy for power generation.

Specifically, publications focus on electrical power production by means of Organic Rankine Cycles (ORCs), either arranged in series or cascade, that use seawater and LNG as heat source and sink, respectively. Yao et al. [20] perform energy and exergy analyses of a simple ORC with several working fluids and they suggest that propane is the most suitable candidate. Lee et al. [21] study the integration of waste heat from engine exhaust gases into the power generation system with cold energy utilisation. The authors, based on the first and second law of the thermodynamics, analyse three configurations: a simple ORC with propane, a two-stage ORC in series with propane in both cycles and a two-stage ORC using the exhaust gases as heat source in the high-temperature cycle. Yoon-Ho [22], based on aforementioned papers, performs a thermo-economic analysis of a simple ORC and a two-stage ORC in series with zeotropic mixtures of ethane and propane. The latter system with pure propane in the high-temperature cycle and an 8:2 ethane/propane mixture in the low-temperature cycle gives the best results. In another publication, Yoon-Ho [23], using pure working fluids, compares ORCs of up to three stages in series isolated and in combination with a turbine that only expands the natural gas (NG) consumed by engines. As an alternative to ORCs in series, Yao et al. [24] evaluate two three-level cascade ORC configurations, while Xu and Lin [25] propose a novel three-level and also a four-level cascade ORC. Both papers aim to increase the exergy efficiency of a conventional three-level cascade ORC.

The exploitation of cold energy to produce power with ORC technology is of interest to companies in the sector [26] since most regasification systems installed on board use seawater to regasify LNG (open loop) either directly or indirectly, that is, performing the heat exchange process through an intermediate fluid [27]. Open-loop regasification systems, however, have been prohibited by certain local authorities owing to the physical and chemical damage caused by the consumption and continual discharge of seawater on the development of marine organisms [28]. Furthermore, these types of systems depend on the environment seawater temperature. Hence, in cold areas the NG temperature is unable to reach the value required for its distribution [29]. The mentioned drawbacks can be solved with the adoption of regasification systems that use the steam generated in boilers as a heat source (closed loop), but fuel consumption and, consequently, CO_2 emission levels drastically increase by comparison to open-loop systems [30]. Moreover, from an exergy standpoint, closed-loop regasification systems not only waste the LNG cold exergy, but also the exergy delivered to the process through the steam generated in the boilers. Therefore, current closed-loop regasification systems require key modifications that allow an efficient use of the steam generated in the boilers and exploitation of the regasification process cold energy in order to significantly reduce CO_2 emissions, and thereby improve FSRU efficiency.

Since no publication has been found in scientific literature that deals with CO_2 capture in FSRUs, nor the exploitation of cold energy in systems that operate in closed loop, the present paper performs an energy, exergy and environmental analysis of a novel closed-loop regasification system that integrates an ORC to fulfil the energy demand of the FSRU, avoiding the use of internal combustion engines, and a carbon-capture system via chemical absorption to significantly reduce CO_2 emission levels deriving from the boiler combustion process. A closed-loop regasification system is proposed capable of operating efficiently in areas where the use of seawater is restricted, with scarcely any CO_2 released into the atmosphere.

2. System description

Fig. 1 is a simplified diagram of the proposed regasification system installed in a typical FSRU with the characteristics of Table 1. The system is then described by the trajectories that the LNG and boil off gas (BOG) follow therein.

LNG stored in the tanks at a pressure slightly above atmospheric and at a temperature of approximately −160 °C is supplied to the regasification system through feed pumps. The LNG then condenses excess BOG (if any) in the recondenser and increases in pressure in the booster pumps to the value required for its subsequent distribution, before entering the ORC. In the latter, the LNG is used as the cold source of the power cycle and the temperature rises to approximately −65 °C. At the ORC outlet it can be considered that the LNG has become regasified NG. Its temperature, however, remains too low: that is, there is still a significant amount of cold energy available. Therefore, the regasified NG from the ORC is taken advantage of to liquefy the CO_2 captured from the boiler flue gases and cool the water-glycol system. The latter allows the safe distribution of cold NG energy required in the cooling processes of CO_2 capture and drying. NG temperature is of approximately 10 °C at the exit of the regasification system.

Similarly, to the feed pumps, low duty (LD) compressors supply the BOG to the recondenser (in case of excess), DF motors and regasification boilers. BOG is the only fuel in regasification boilers for saturated steam generation at 29 bar. This high-pressure steam is used directly in the ORC as a hot source, although it needs to be decreased in pressure and saturated for use in the desorption process of the CO_2 capture system. In this system, the flue gases treated through the absorption process and

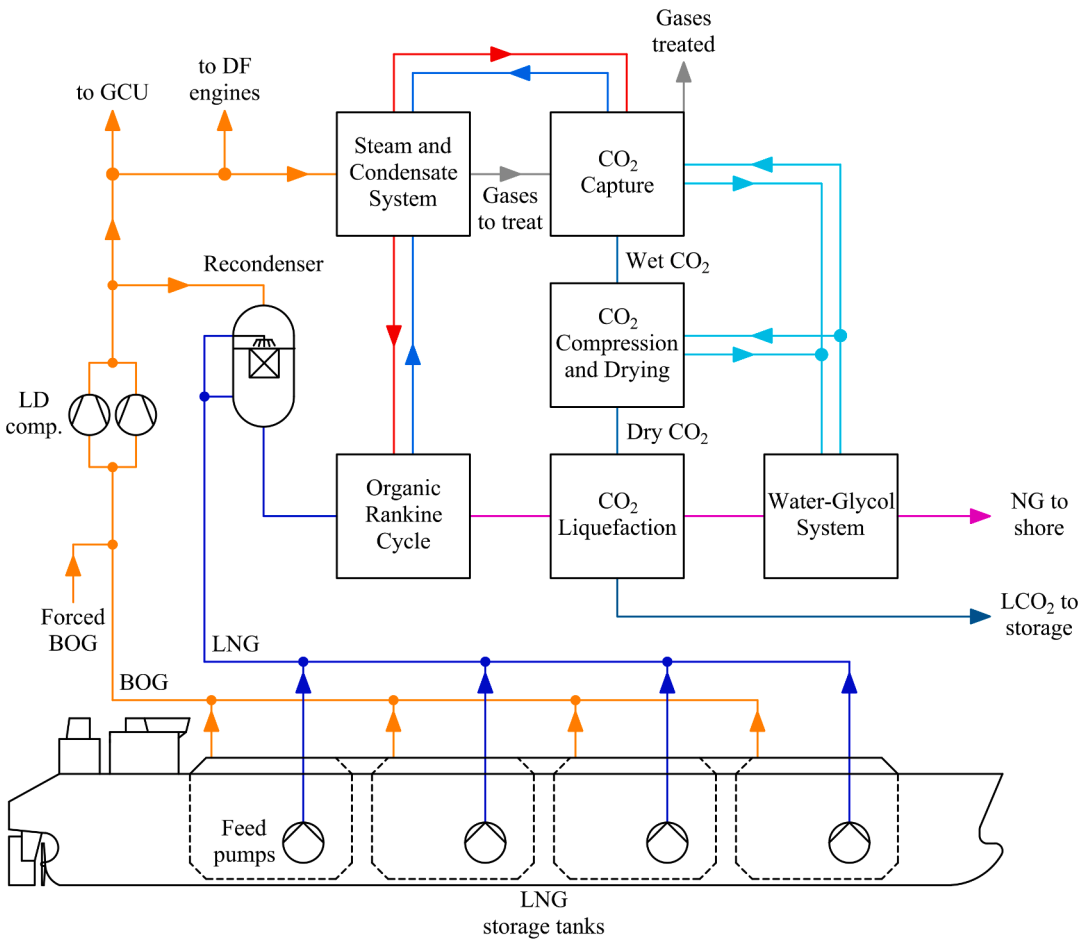

Fig. 1. Simplified scheme of the proposed closed loop regasification system integrating the ORC and the CO_2 capture, treatment and liquefaction processes.

Table 1
General specifications of the model FSRU.

Item	Value
Type of LNG storage tanks	MARK III, maximum vapour pressure of 0.7 bar(g) and boil off rate (BOR) of 0.15%
Cargo capacity	170 000 m^3
Type of LD compressor	2 stage centrifugal compressor with pre-cooling
Maximum / baseload regasification capacity	750 mmscfd / 500 mmscfd
Propulsion system	Dual fuel diesel electric (DFDE)
Engines	3 × Wärtsilä 12V50DF (11.4 MW) 1 × Wärtsilä 6L50DF (5.7 MW)

without CO_2 are released directly into the atmosphere at a temperature of 40–42 °C, while the CO_2 given off in the desorption process (wet CO_2) must be compressed and dried (reduce water content) for the subsequent CO_2 liquefaction process (approx. −50 °C). The liquefied CO_2 (LCO_2) can then be temporarily stored in the FSRU -which would involve installing storage tanks on board- or directly offloaded to storage tanks on shore.

The following subsections further describe each of the aforementioned subsystems of the regasification system.

2.1. Steam and condensate system with ORC

The steam and condensate system with ORC is illustrated in Fig. 2. The processes that the system entails are described below.

LNG discharged by feed pump (P-1) is supplied to the recondenser (R) through valve (V-1), which simulates pressure drops up to the recondenser inlet. The LNG is then driven by booster pump (P-2) towards the vaporizer (VP). Herein, while the LNG increases in temperature and evolves to supercritical state, the propane vapour from the exhaust of the turbine (T) condenses until reaching saturated liquid state. Next, the liquid propane is driven by pump (P-3) towards the vaporizer (PVP), where it reaches the state of saturated vapour required to drive the turbine and satisfy the power demand of the FSRU.

In the propane vaporizer, the high pressure steam flow rate regulated by valve (V-3) condenses and returns in liquid state through valve (V-4) to the feed tank (FT). The feed water flow rate required by the boiler -supplied by water pump (P-4)- increases in temperature to 135 °C in the preheater (PH). Steam used in heating processes other than the ORC is supplied through valve (V-5), which reduces the pressure of the steam coming from the boiler to 9 bar. The 9 bar steam is used directly in the preheater and feed tank coil, returning the condensate through steam traps (T-1 and T-2). In the case of the CO_2 capture system desorption process, the heating steam must be saturated at 3.5 bar. The condensate from the steam traps is cooled in the drain cooler/condenser (DC) and returns to the feed tank, closing the steam-condensate circuit.

The fuel required to meet the energy demand of the FSRU comes from the BOG generated naturally in the tank and the LNG vaporized in the forcing vaporizer (FV). The fuel gas pump is responsible for supplying LNG to the forcing vaporizer and to the BOG pre-cooling process in the mixer (MX). Any liquid content is removed from the BOG cooled to a temperature of −120 °C in the mist separator (S-1) before increasing in pressure in the LD compressor. Any surplus BOG generated in the tank is condensed in the recondenser through valve (V-2). The BOG used as fuel is conditioned in the after cooler/NG heater (AC/NGH). As the system is designed for the ORC to meet the FSRU's power demand

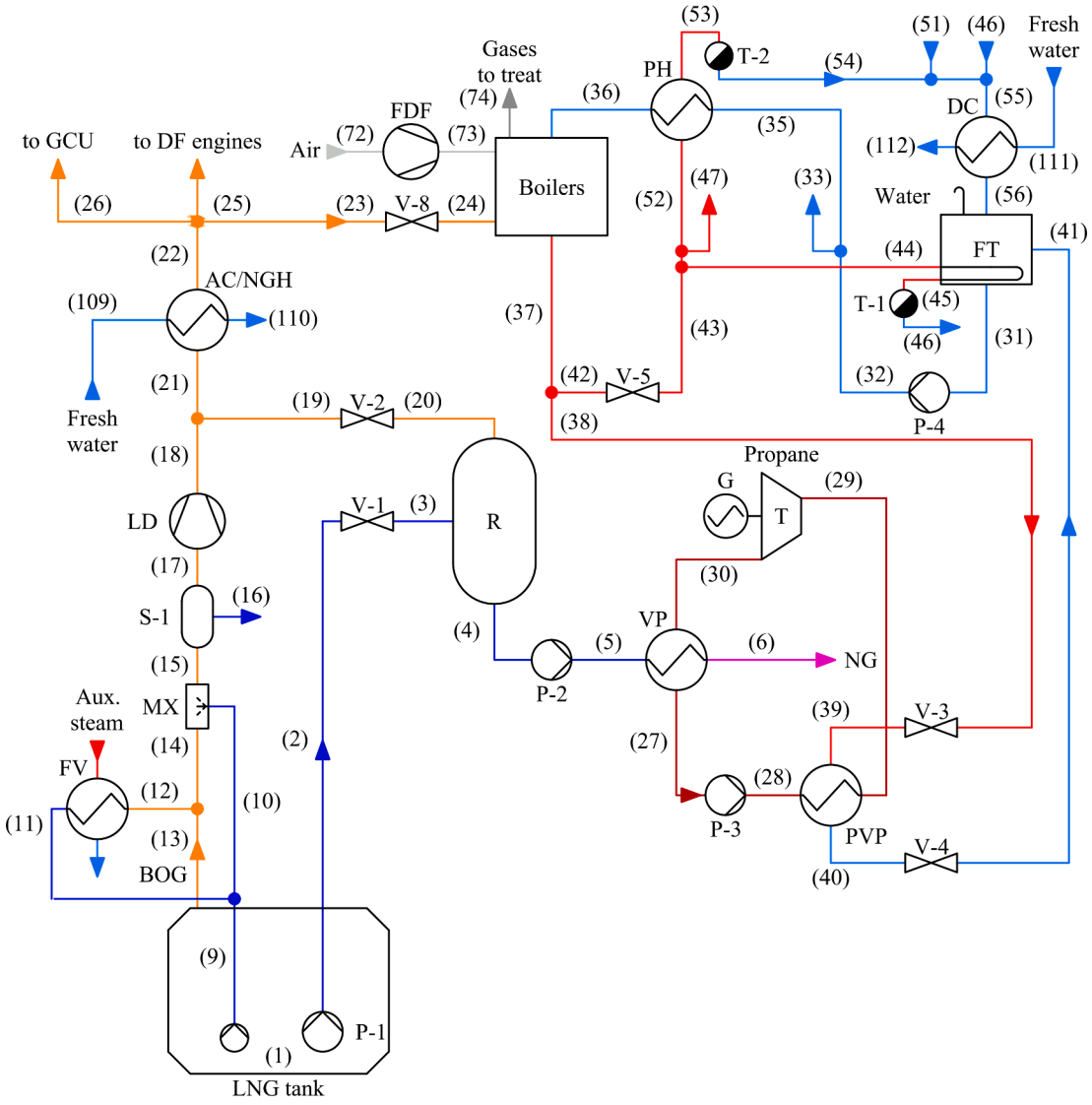

Fig. 2. Diagram of the steam and condensate system with ORC.

during the regasification process, BOG consumption is exclusively attributed to the boiler; fuel is supplied through valve (V-8), while air is supplied by the forced draft fan (FDF). The gases produced in combustion are treated in the CO_2 capture system.

2.2. *Post-combustion CO_2 capture with chemical absorption*

Fig. 3 depicts the CO_2 capture system with chemical absorption and a description follows below.

Boiler flue gases are cooled in the heat exchanger with water-glycol (WGH-1) to an adequate temperature for the absorption process (approx. 40 °C). Under these conditions, the temperature of the gases is below dew point, and so the condensed water needs to be removed in phase separator (S-2) before driving the gases through the absorber (ABS) by means of the flue gas blower (FGB).

In the absorber, the gases are brought into counter-current contact with the CO_2-lean MEA aqueous solution, where the CO_2 of the gases reacts with the solution to form bicarbonate and carbamate. Thus, the treated gases, that is, practically CO_2-free gases, exit the upper part of the column directly into the atmosphere, while the CO_2-rich solution extracted from the lower part is driven by pump (P-6) towards the stripper (STR). Next, the rich solution increases in temperature to 105 °C in the heat exchanger (RMH) with the lean solution from the reboiler (REB) in order to reduce the flow rate of saturated steam supplied to the latter by the desuperheater (DSH-1) via the water (V-6) and steam (V-7) valves. Subsequently, the heated rich solution enters the regenerator through valve (V-9), while the lean solution drops in temperature to 40 °C in water-glycol heat exchanger (WGH-2). The cooled lean solution returns to the absorber through valve (V-10). It must first, though, be filled with MEA and water to offset the losses incurred in the capture process.

In the regenerator, vapour exiting the upper part of the column drops in temperature to 40 °C in the condenser (COND), while the liquid removed from the bottom proceeds to the reboiler. In here, the liquid from the regenerator is partially vaporized at an approximate temperature of 120 °C and the phases are separated: the liquid phase, a CO_2-lean solution that is driven by pump (P-7) towards the rich-solution heater; and the vapour phase rich in CO_2 that returns to the regenerator. With regard to the condenser, the fluid at the outlet is in wet vapour state, where the vapour phase is mainly composed of CO_2, and the liquid phase is essentially water. Thus, to obtain CO_2, the vapour-liquid mixture must be subjected to a phase separation process in

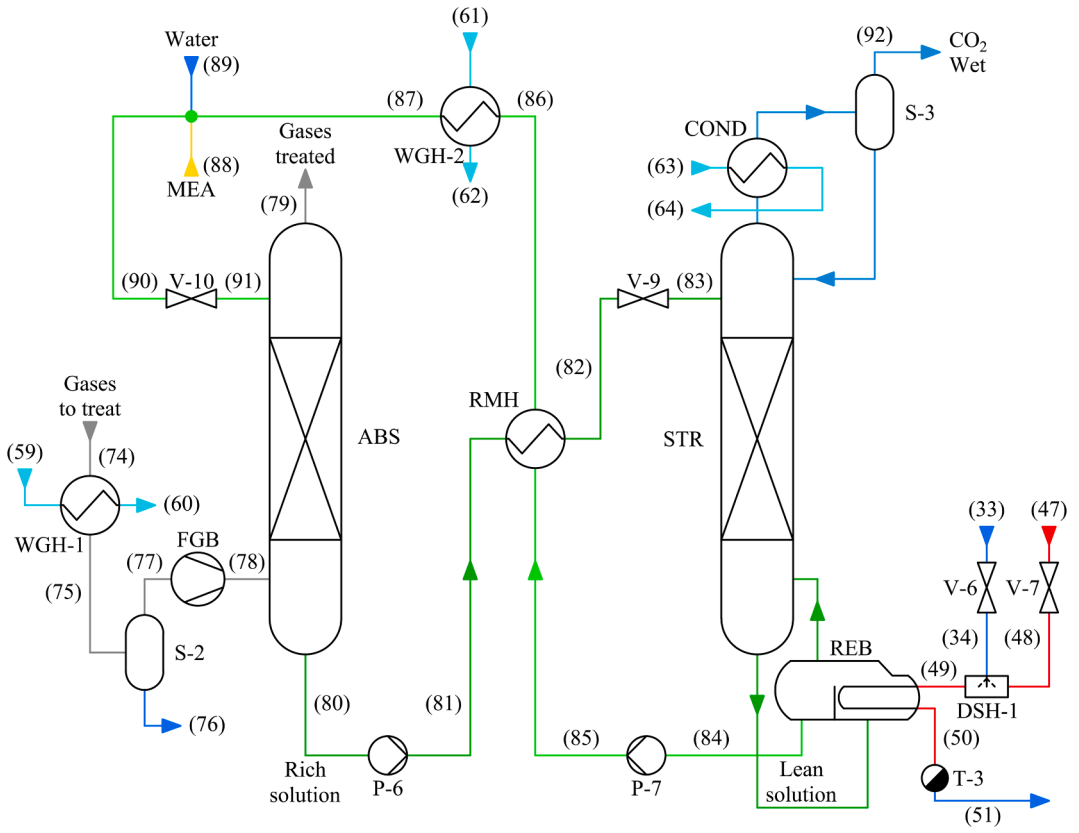

Fig. 3. Diagram of the post-combustion CO_2 capture with chemical absorption.

separator (S-3). The liquid phase extracted during the separation process is returned entirely to the regenerator, while the captured CO_2 -which still has a high water content (wet CO_2)- is subjected to the compression and drying process.

2.3. CO_2 compression and drying

The compression and drying process of the wet CO_2 from the chemical absorption capture system is illustrated in Fig. 4. This process requires the combination of refrigeration and adsorption drying to avoid possible freezing problems in CO_2 liquefaction. Additionally, the state change process requires gas pressure to be above triple point (5.17 bar). Therefore, CO_2 compression is carried out in two stages with intermediate cooling to reduce power demand. The drying and compression process is further described below.

The wet CO_2 in saturated vapour state at 40 °C drops in temperature in water-glycol heat exchanger (WGH-3) to 3 °C. Subsequently, the liquid phase -mainly comprising water- is removed in phase separator (S-4), while the condensate-free CO_2 heads toward the first compression stage (C-1). Between the two compression stages the CO_2 is re-cooled to a temperature of 3 °C through water-glycol exchanger (WGH-4) and the condensed water is removed in phase separator (S-5) before the second compression stage (C-2). The compressed CO_2 then undergoes the final cooling and separation process with water-glycol exchanger (WGH-4) and phase separator (S-6). Lastly, the CO_2 enters the adsorber (ADS), where the dew point drastically drops to a value below the liquefaction

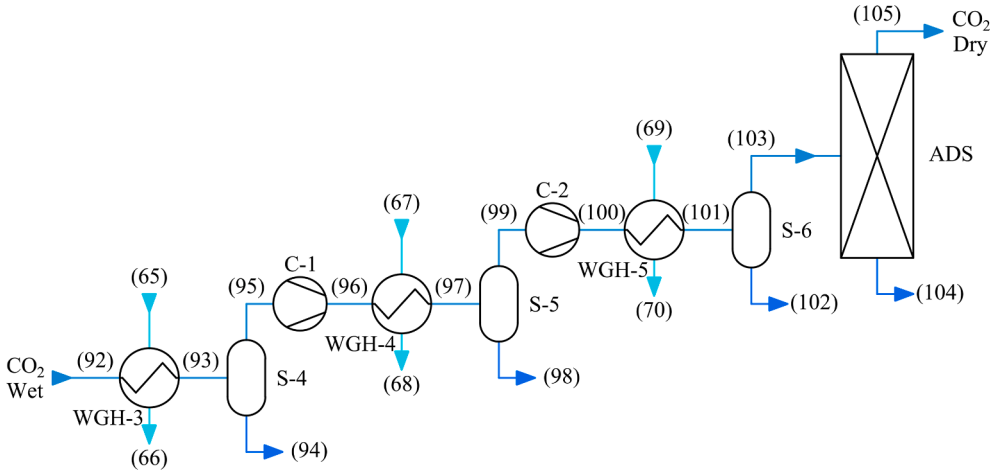

Fig. 4. Diagram of the CO_2 compression and drying process.

process temperature (approx. −55 °C). In order to reduce the dew point temperature to values under −60 °C, adsorption drying requires the use of molecular sieves.

2.4. CO_2 liquefaction and water-glycol system

The CO_2 liquefaction process and the water-glycol system that distributes the LNG cold energy to the cooling processes of the capture and drying systems are illustrated in Fig. 5 and described below.

Dry CO_2 changes phase in liquefier (LCO2), where heat exchange takes place with NG from the ORC. The CO_2 temperature at the outlet of this component can be adjusted to remove gases with a boiling point under that of CO_2 (non-condensing gases) in phase separator (S-7) and increase the purity of the stored LCO_2. During the CO_2 liquefaction process, the NG slightly increases in temperature and continues to the final heating process prior to delivery to land. Next, the NG temperature reaches a value of approximately 10 °C in the water-glycol cooler (WGC), while the water-glycol mixture from the water-glycol heaters (WGHs) at 15 °C decreases in temperature to −5 °C. The water-glycol circuit pressure drops are offset via pump (P-5), which increases the fluid pressure and allows for the distribution of LNG cold energy to all processes that require cooling in the regasification system.

3. Mathematical modelling

The conditions assumed in the study of the proposed regasification system are presented below:

- Steady-state and adiabatic (no heat exchange with the environment) condition for all components except the cargo tanks. The potential and kinetic effects are neglected in the energy and exergy balances.
- The Peng-Robinson equation of state is used to calculate the properties of the fluids in the regasification system with some exceptions. The IAPWS-IF97 and Acid Gas - Chemical Solvents packages are applied respectively in the steam/condensate system and in the CO_2 capture with chemical absorption.
- The LNG reference composition is 100% methane with a lower heating value of 49 500 kJ/kg. Table 2 shows the composition of a measured LNG for comparison purposes.
- The concentration on a mass basis of ethylene glycol in water is of 30%.
- The air composition on a molar basis is of 21% oxygen and 79% nitrogen.

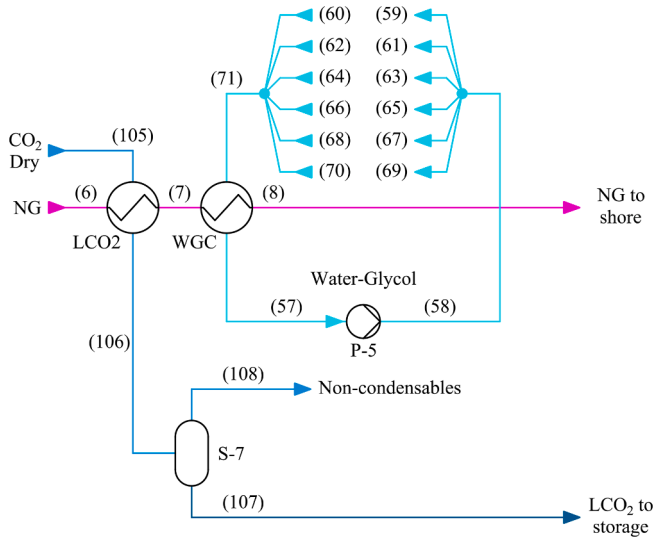

Fig. 5. Diagram of the CO_2 liquefaction process and water-glycol system.

Table 2
NG composition measured on board an FSRU.

Component	Mole fraction
Methane (CH_4)	0.89018
Nitrogen (N_2)	0.00007
Carbon dioxide (CO_2)	0.00000
Ethane (C_2H_6)	0.07974
Propane (C_3H_8)	0.02291
i-Butane (i-C_4H_{10})	0.00322
n-Butane (n-C_4H_{10})	0.00371
i-Pentane (i-C_5H_{12})	0.00014
n-Pentane (n-C_5H_{12})	0.00002
n-Hexane (n-C_6H_{14})	0.00001

- Negligible auxiliary boiler fuel consumption.
- The CO_2 emission factor for NG is 2.750 g CO_2/g fuel [31].
- The ORC provides all the FSRU's electricity demand. The power consumption of auxiliary services is 2050.9 kW, exempting the components of the regasification system.
- The compression ratio for C-1 and C-2 is the same.
- The regasification system is designed for a CO_2 capture efficiency of at least 90.00%.
- Tables 3–8 contain the main parameters applied.

The following subsections provide a description of the mathematical models and analyses developed to study the regasification system.

3.1. BOG generation in the LNG storage tanks

Although LNG storage tank insulation is designed to limit heat transfer from the environment, some of the cargo naturally vaporizes due to the small heat input. The natural BOG mass flow rate ($\dot{m}_{BOG,n}$) can be calculated as [32]:

$$\dot{m}_{BOG,n} = BOR V_{tk} \rho_{LNG} \quad (1)$$

where BOR is the boil-off rate, V_{tk} is the total cargo capacity and ρ_{LNG} is the LNG density.

During the regasification process, BOG generated in the tanks is continually removed, as is the LNG required to supply the FSRU's energy demand (fuel gas pump) and the LNG supplied to the regasification system (feed pump). In this non-stationary process, the tank volume remains constant. Therefore, as the liquid-zone volume decreases, the vapour-zone volume increases [33]. Given the assumption that the thermodynamic properties remain uniform in each of the mentioned zones, the BOG extracted from the tank ($\dot{m}_{BOG}$) is determined with the following equation [34]:

Table 3
General parameters assumed for the regasification system.

Parameter	Value
LNG tank pressure	1.16325 bar
BOG temperature from tank	−100 °C
Regasified NG mass flow rate	111.19 kg/s
Regasified NG pressure	85 bar
Regasified NG temperature	10 °C
Pumps, fans and compressors isentropic efficiency	80%
Pumps, fans and compressors electromechanical efficiency	90%
Feed pump discharge pressure	9 bar
Booster pump discharge pressure	110 bar
LD isentropic efficiency	55%
LD electromechanical efficiency	80%
BOG temperature after the mixer	−120 °C
LD discharge pressure	6 bar
Recondenser pressure	5.5 bar
Minimum temperature difference in heat exchangers	5 °C
NG pressure drop through the vaporizer	21 bar
NG pressure drop through the LCO2	2 bar

Table 4
Parameters assumed for the ORC.

Parameter	Value
Propane pump suction pressure	1.5 bar
Propane pressure drop in heat exchangers	0.5 bar
Propane vapour quality at the propane vaporizer outlet	1
Expander isentropic efficiency	80%
Expander electromechanical efficiency	90%

Table 5
Parameters assumed for the steam/condensate system.

Parameter	Value
Force draft fan pressure increase	0.05 bar
Boiler efficiency	90%
Excess air	10%
Water pressure at the feed tank	1.01325 bar
Water temperature at the feed tank	90 °C
Water temperature at the pre-heater outlet	135 °C
Saturation pressure at steam dome	29 bar
Steam pressure at the propane vaporizer inlet	25.5 bar
Water pressure at the propane vaporizer outlet	2.5 bar
Water temperature at the propane vaporizer outlet	30.02 °C
Heating steam pressure	9 bar
Heating steam pressure after DSH-1	3.5 bar
Heating steam temperature after DSH-1	140 °C
Water temperature at the condenser outlet	90 °C

Table 6
Parameters assumed for the carbon capture system.

Parameter	Value
MEA mass concentration in lean amine solution	30%
MEA and water temperature (make up)	40 °C
MEA and water pressure (make up)	3 bar
Flue gas temperature after WGH-1	40 °C
Flue gas blower pressure increase	0.05 bar
Amine solution pumps pressure discharge	4 bar
Lean amine solution temperature after RMH	105 °C
Amine solution pressure drop in heat exchangers	0.5 bar
Stripper pressure	2 bar
Stripper condenser temperature	40 °C
Absorber and stripper packing type	Mellapak 250 Y
Absorber and stripper stage packing height	0.500 *m*
Absorber/stripper stages	14/10

Table 7
Parameters assumed for the CO_2 compression and drying.

Parameter	Value
CO_2 temperature after water-glycol heat exchangers	3 °C
CO_2 pressure drop in heat exchangers	0.5 bar
Pressure discharge of the C-2	7.5 bar
CO_2 water molar fraction after the adsorber	10^{-6}

Table 8
Parameters assumed for the water-glycol system.

Parameter	Value
Water-glycol pump suction pressure	3.5 bar
Water-glycol pump discharge pressure	6 bar
Water-glycol pressure drop in WGHs	0.5 bar
Water-glycol temperature at the WGC inlet	15 °C
Water-glycol temperature at the WGC outlet	−5 °C

$$\dot{m}_{BOG} = \dot{m}_{BOG,n} - \frac{v_{LNG}}{v_{BOG}}\left(\dot{m}_{LNG} + \dot{m}_{BOG,n}\right) \quad (2)$$

where v_{LNG} is the LNG specific volume, v_{BOG} is the BOG specific volume and $\dot{m}_{LNG}$ is the mass flow rate of LNG removed from the tank.

Eqs. (1) and (2) were entered into the Aspen HYSYS using a Spreadsheet object in order to simulate BOG generation in LNG storage tanks.

3.2. Simulation of the CO_2 capture system using aqueous MEA

The CO_2 capture system developed in Aspen HYSYS applies the Acid Gas - Chemical Solvents property package to simulate absorption and stripping processes with the aqueous MEA solution in the treatment of flue gases from the boiler. This package uses different thermodynamic models for the vapour and liquid phases: the Peng-Robinson equation of state is applied in the vapour phase, while the electrolyte non-random two-liquid (e-NRTL) activity coefficient model is applied in the liquid phase [35]. The range of validity of the vapour-liquid equilibrium to simulate the processes with aqueous solutions of MEA is depicted in Table 9. Table 10 shows the reactions applied by the properties package to simulate the formation of electrolytes in the solution and the absorption and desorption processes.

In terms of absorber and regenerator simulation, the Aspen HYSYS has two non-equilibrium calculation methods: Efficiency and Advanced Modelling [36]. The Efficiency method first uses a conventional equilibrium-stage model to solve the columns and then models the non-equilibrium behaviour by calculating a rate-based efficiency for CO_2 at each stage. By contrast, the Advanced Modelling method employs Maxwell-Stefan theory to rigorously calculate heat flow and mass transfer without assuming equilibrium conditions between the liquid and vapour at each stage. The Efficiency method convergence tends to occur quickly and offers similar results to the Advanced Modelling method [37]. Given the complexity of the proposed regasification system, the Efficiency method has been applied to simulate absorption and desorption processes. Table 11 lists the conditions applied in the solver for the absorber and regenerator.

To build the model in Aspen HYSYS, the CO_2 capture system requires a Recycle block to feed back the flow rate of aqueous lean amine solution coming from the regenerator towards the absorber and a Make-up object for the filling of MEA and water.

3.3. Energy analysis

The first law of thermodynamics establishes the principle of energy conservation and relates the energy change of a system to the heat and power transferred through it. Therefore, the energy balance applied to any steady state control volume, neglecting kinetic and potentials effects, is defined by the following equation:

$$\dot{Q} - \dot{W} + \sum_i \dot{m}_i h_i - \sum_o \dot{m}_o h_o = 0 \quad (3)$$

where $\dot{Q}$ is the heat flow rate transferred to the control volume (positive sign), $\dot{W}$ is the power developed by the control volume (positive sign) and $\sum_i \dot{m}_i h_i - \sum_o \dot{m}_o h_o$ is the enthalpy change between the inlet and outlet mass flow rates of the control volume.

The energy balances under adiabatic condition derived from Eq. (3) for pumps and compressors (including fans); turbine; valves; desuperheater, mixer and recondenser; phase separators; and heat

Table 9
Validity range of the vapour-liquid equilibrium for MEA in Aspen HYSYS [36].

Temperature (K)	Pressure (kPa)	Amine (mole fraction)	CO_2 loading
273–443	0.001–20 000	0.06–0.16	0.002–1.33

Table 10
Electrolyte solution chemistry and kinetic reactions for carbon capture system with MEA [36].

Reaction name	Reaction	Type
Water dissociation	$2H_2O \leftrightarrow H_3O^+ + OH^-$	Equilibrium
CO_2 hydrolysis	$CO_2 + 2H_2O \leftrightarrow HCO_3^- + H_3O^+$	Equilibrium
Bicarbonate dissociation	$HCO_3^- + H_2O \leftrightarrow CO_3^{2-} + H_3O^+$	Equilibrium
MEA protonation	$MEAH^+ + H_2O \leftrightarrow MEA + H_3O^+$	Equilibrium
Carbamate hydrolysis	$MEACOO^- + H_2O \leftrightarrow MEA + HCO_3^-$	Equilibrium
Bicarbonate formation (forward)	$CO_2 + OH^- \rightarrow HCO_3^-$	Kinetic
Bicarbonate formation (reverse)	$HCO_3^- \rightarrow CO_2 + OH^-$	Kinetic
Carbamate formation (forward)	$MEA + CO_2 + H_2O \rightarrow MEACOO^- + H_3O^+$	Kinetic
Carbamate formation (reverse)	$MEACOO^- + H_3O^+ \rightarrow MEA + CO_2 + H_2O$	Kinetic

Table 11
Definition of solver characteristics for absorber and stripper.

Solving Method	Maximum number of iterations	Equilibrium error tolerance	Heat error tolerance	Damping
Modified HYSYM Inside-Out	10 000	10^{-6}	10^{-6}	Adaptative

exchangers are respectively:

$$\dot{W}_{\text{pump/comp}} = \dot{m}(h_o - h_i) \tag{4}$$

$$\dot{W}_{\text{turb}} = \dot{m}(h_i - h_o) \tag{5}$$

$$h_i = h_o \tag{6}$$

$$\sum_i \dot{m}_i h_i = \dot{m}_o h_o \tag{7}$$

$$\dot{m}_i h_i = \sum_o \dot{m}_o h_o \tag{8}$$

$$\sum_i \dot{m}_i h_i = \sum_o \dot{m}_o h_o \tag{9}$$

Regarding to the combustion reaction in the boiler, Eq. (10) establishes the energy balance as:

$$(\eta_{\text{comb}} - \eta_{\text{b}})\left(h_{\text{LHV,BOG}}\right) M_{\text{BOG,b}} = \sum_{\text{P}} n_o(\Delta\bar{h}_o) - \sum_{\text{R}} n_i(\Delta\bar{h}_i) \tag{10}$$

where η_{comb} is the combustion efficiency, η_{b} is the boiler efficiency, $M_{\text{BOG,b}}$ is the molar mass of BOG consumed by the boiler and the other side of the equation represents the molar enthalpy change between the products and reactants.

The η_{b} is defined by the following equation:

$$\eta_{\text{b}} = \frac{\dot{Q}_{\text{b}}}{\dot{m}_{\text{BOG,b}} h_{\text{LHV,BOG}}} \tag{11}$$

where $\dot{Q}_{\text{b}}$ is the heat flow rate of the boiler, $\dot{m}_{\text{BOG,b}}$ is the BOG mass flow rate consumed by the boiler and $h_{\text{LHV,BOG}}$ is the lower heating value of BOG.

The regasification system power demand ($\dot{W}_{\text{RS}}$) can be determined as:

$$\dot{W}_{\text{RS}} = \sum \dot{W}_{\text{pump}} + \sum \dot{W}_{\text{comp}} \tag{12}$$

However, Eq. (12) does not consider the electromechanical efficiency ($\eta_{\text{el,m}}$) of the electrical consumption equipment. Thus, in order to determine the FSRU's electrical demand, the electrical power required by each pump or compressor ($\dot{W}_{\text{el,pump/comp}}$) must be calculated as:

$$\dot{W}_{\text{el,pump/comp}} = \frac{\dot{W}_{\text{pump/comp}}}{\eta_{\text{el,m}}} \tag{13}$$

Therefore, the FSRU's electrical demand ($\dot{W}_{\text{el,FSRU}}$) is:

$$\dot{W}_{\text{el,FSRU}} = \dot{W}_{\text{el,b}} + \sum \dot{W}_{\text{el,pump}} + \sum \dot{W}_{\text{el,comp}} \tag{14}$$

where $\dot{W}_{\text{el,b}}$ represents the electrical consumption of the ship's auxiliary services, including the fuel gas pump.

The power developed by the turbine ($\dot{W}_{\text{turb}}$), calculated with Eq. (5), must satisfy the electrical balance of the FSRU as the following equation implies:

$$\dot{W}_{\text{turb}} = \frac{\dot{W}_{\text{el,FSRU}}}{\eta_{\text{alt}}} \tag{15}$$

where η_{alt} is the efficiency of the alternator.

The total energy flow rate supplied to the FSRU ($\dot{H}_{\text{tot}}$) is defined as:

$$\dot{H}_{\text{tot}} = \dot{m}_{\text{BOG,b}} h_{\text{LHV,BOG}} \tag{16}$$

The energy efficiency of an FSRU can be measured based on the specific energy consumption (b_{FSRU}) as:

$$b_{\text{FSRU}} = \frac{\dot{H}_{\text{tot}}}{\dot{m}_{\text{NG}}} \tag{17}$$

where $\dot{m}_{\text{NG}}$ is the regasified NG mass flow rate.

3.4. Exergy analysis

Exergy analysis, which combines the first and second laws of thermodynamics, allows determining the destruction of exergy (useful work) caused by the irreversibilities of the equipment. It is, therefore, a more convenient method than energy analysis when defining efficiencies and identifying possible improvements from a thermodynamic standpoint. The exergy rate of a material stream ($\dot{E}$) is defined by:

$$\dot{E} = \dot{m}e = \dot{m}\left(e^{\text{ph}} + e^{\text{ch}}\right) \tag{18}$$

where e^{ph} is the specific physical exergy and e^{ch} is the specific chemical exergy.

The specific physical exergy is calculated as:

$$e^{\text{ph}} = h - h_0 - T_0(s - s_0) \tag{19}$$

where the subscript 0 refers to the pressure and temperature conditions of the dead state.

In this analysis, the physical exergy terms of NG must be explored in order to define the exergy efficiency of the FSRU. Therefore, physical exergy is decomposed into a thermal (e^{th}) and a mechanical (e^{p}) component with the following equations [38]:

$$e^{\text{ph}} = e^{\text{th}} + e^{\text{p}} \tag{20}$$

$$e^{\text{th}} = e^{\text{ph}}(T, p) - e^{\text{ph}}(T_0, p) \tag{21}$$

$$e^{\text{p}} = e^{\text{ph}}(T_0, p) - e^{\text{ph}}(T_0, p_0) \tag{22}$$

The standard chemical exergies of the pure substances used in this study are listed in Table 12. Propane and ethylene glycol substances are disregarded as they do not participate in any reactive process or change in composition. In the case of MEA, the standard chemical exergy is calculated from its chemical formula using the group contribution method [39]:

Table 12
Standard chemical exergy of fluids [39].

Substance	Standard chemical exergy	
	(kJ/kmol)	(kJ/kg)
Carbon dioxide	19 870.00	451.49
MEA	1 535 970.00	25 145.33
Nitrogen	720.00	25.70
Oxygen	3970.00	124.07
Water (gas)	9500.00	527.31
Water (liquid)	900.00	49.96

$$\overline{e}^{\mathrm{ch}} = \sum_i g_i \overline{e}^{\mathrm{ch}}_{\mathrm{g},i} \tag{23}$$

where g_i is the number of each group and $\overline{e}^{\mathrm{ch}}_{\mathrm{g},i}$ is the chemical exergy of each group.

The specific chemical exergy coincides with the standard chemical exergy value for a pure substance. With mixtures, however, the effect of the mixing process must be taken into account. Generally, the specific chemical exergy (e^{ch}) for any two-phase pure substance or mixture can be defined as [40]:

$$e^{\mathrm{ch}} = \frac{1}{M}\left(y_{\mathrm{g}}\overline{e}^{\mathrm{ch}}_{\mathrm{g}} + y_{\mathrm{l}}\overline{e}^{\mathrm{ch}}_{\mathrm{l}}\right) \tag{24}$$

where M is the molar mass, y_{g} is the mole fraction of the gas phase, $\overline{e}^{\mathrm{ch}}_{\mathrm{g}}$ is the molar chemical exergy of the gas phase, y_{l} is the mole fraction of the liquid phase and $\overline{e}^{\mathrm{ch}}_{\mathrm{l}}$ is the molar chemical exergy of the liquid phase.

The molar chemical exergy for each of the phases is calculated using the following equation [41]:

$$\overline{e}^{\mathrm{ch}} = \sum_i y_i \overline{e}^{\mathrm{ch}}_i + \Delta\overline{e}^{\mathrm{m}} \tag{25}$$

where $\overline{e}^{\mathrm{ch}}_i$ is the standard chemical exergy of each pure substance and $\Delta\overline{e}^{\mathrm{m}}$ is the exergy of mixing.

The exergy of mixing is given by the Gibbs energy of the mixing process ($\Delta\overline{g}^{\mathrm{m}}_0$) at temperature T_0 and pressure p_0, which is calculated from the enthalpy ($\Delta\overline{h}^{\mathrm{m}}$) and entropy ($\Delta\overline{s}^{\mathrm{m}}$) of mixture through the equations below [41]:

$$\Delta\overline{e}^{\mathrm{m}} = \Delta\overline{g}^{\mathrm{m}}_0 = (\Delta\overline{h}^{\mathrm{m}} - T_0\Delta\overline{s}^{\mathrm{m}}) \tag{26}$$

$$\Delta\overline{h}^{\mathrm{m}} = \overline{h}^{\mathrm{m}} - \sum_i y_i \overline{h}_i \tag{27}$$

$$\Delta\overline{s}^{\mathrm{m}} = \overline{s}^{\mathrm{m}} - \sum_i y_i \overline{s}_i \tag{28}$$

where $\overline{h}^{\mathrm{m}}$ is the molar enthalpy of formation of the mixture, $\overline{h}_i$ is the molar enthalpy of formation of each pure substance present in the mixture, $\overline{s}^{\mathrm{m}}$ is the standard molar entropy of the mixture and $\overline{s}_i$ is the standard molar entropy of each pure substance.

Eqs. (24), (25), (26), (27) y (28) are applied to determine the specific chemical exergy of all the relevant states, with the exception of those involving NG. The chemical exergy of NG is [39]:

$$e^{\mathrm{ch}} = \varphi h_{\mathrm{LHV}} \tag{29}$$

where φ is the NG exergy factor with a value of 1.04.

The exergy destroyed ($\dot{I}$) by pumps and compressors; turbine; valves; desuperheater, mixer and recondenser; heat exchangers; as well as the boiler are determined respectively with Eqs. (30), (31), (32), (33), (34) and (35). With regard to the phase separators, the exergy destroyed is considered null, since they do not undergo any change in temperature or pressure during the separation process.

$$\dot{I}_{\mathrm{pump/comp}} = \dot{W}_{\mathrm{pump/comp}} - \dot{m}(e_o - e_i) \tag{30}$$

$$\dot{I}_{\mathrm{turb}} = \dot{m}(e_i - e_o) - \dot{W}_{\mathrm{turb}} \tag{31}$$

$$\dot{I}_{\mathrm{valve}} = \dot{m}(e_i - e_o) \tag{32}$$

$$\dot{I}_{\mathrm{DSH/MX/R}} = \sum_i \dot{m}_i e_i - \dot{m}_o e_o \tag{33}$$

$$\dot{I}_{\mathrm{heatexchanger}} = \sum_i \dot{m}_i e_i - \sum_o \dot{m}_o e_o \tag{34}$$

$$\dot{I}_{\mathrm{boiler}} = \left[\left(\dot{m}_{\mathrm{air}} e_{\mathrm{air}} + \dot{m}_{\mathrm{BOG,b}} e_{\mathrm{BOG,b}}\right) - \dot{m}_P e_P\right] - \left[\dot{m}_{\mathrm{water}}(e_o - e_i)\right] \tag{35}$$

The exergy efficiency of pumps and compressors is:

$$\eta_{\mathrm{ex,pump/comp}} = \frac{\dot{m}(e_o - e_i)}{\dot{W}_{\mathrm{pump/comp}}} \tag{36}$$

The exergy efficiency of the turbine can be defined as:

$$\eta_{\mathrm{ex,turb}} = \frac{\dot{W}_{\mathrm{turb}}}{\dot{m}(e_i - e_o)} \tag{37}$$

The exergy efficiency of heat exchangers is determined as follows:

$$\eta_{\mathrm{ex,heatexchanger}} = \frac{[\dot{m}(e_o - e_i)]_{\mathrm{product}}}{[\dot{m}(e_i - e_o)]_{\mathrm{supply}}} \tag{38}$$

Eq. (38) is applicable to the desuperheater, mixer (pre-cooling) and recondenser as they operate as open heat exchangers.

The exergy efficiency of the boiler can be defined as:

$$\eta_{\mathrm{ex,boiler}} = \frac{\dot{m}_{\mathrm{water}}(e_o - e_i)}{\left(\dot{m}_{\mathrm{air}} e_{\mathrm{air}} + \dot{m}_{\mathrm{BOG,b}} e_{\mathrm{BOG,b}}\right) - \dot{m}_P e_P} \tag{39}$$

Valves and steam traps, as dissipative components, are combined with the nearest heat exchangers to determine the exergy efficiency of the subsystem.

3.5. Exergy efficiency of the ORC

Exergy flow rates involved in power generation of the ORC are shown in Fig. 6.

The exergy balance equation of the ORC is:

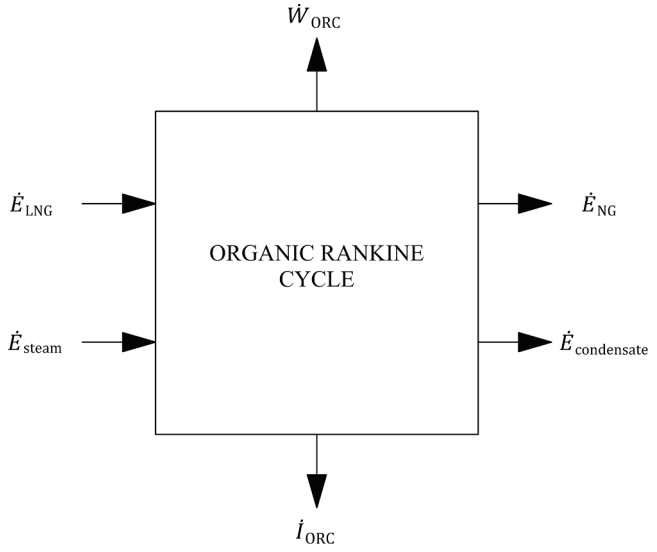

Fig. 6. Exergy balance of the ORC.

$$\dot{I}_{ORC} = \left(\dot{E}_{LNG} - \dot{E}_{NG}\right) + \left(\dot{E}_{steam} - \dot{E}_{condensate}\right) - \dot{W}_{ORC} \quad (40)$$

where $\dot{I}_{ORC}$ is the exergy destroyed due to irreversibilities, $\dot{E}_{LNG}$ is the exergy flow rate of the LNG from the booster pump, $\dot{E}_{NG}$ is the NG exergy flow rate at the ORC outlet and $\dot{W}_{ORC}$ is the net power produced by the ORC.

The ORC uses the steam produced in the boiler and the LNG cold energy for power generation. Therefore, the exergy efficiency of the ORC ($\eta_{ex,ORC}$) is defined as:

$$\eta_{ex,ORC} = \frac{\dot{W}_{ORC}}{\left(\dot{E}_{LNG} - \dot{E}_{NG}\right) + \left(\dot{E}_{steam} - \dot{E}_{condensate}\right)} \quad (41)$$

3.6. Exergy efficiency of the carbon capture system

Fig. 7 provides a graphic illustration of the exergy flow rates involved in the CO_2 capture process.

The exergy balance of the CO_2 capture system is:

$$\dot{I}_{CC} + \dot{E}_{water} = \left(\dot{E}_{g,inlet} - \dot{E}_{g,outlet}\right) + \left(\dot{E}_{MEA} + \dot{E}_{water}\right)_{makeup} + \left(\dot{E}_{WG,inlets} - \dot{E}_{WG,outlets}\right) + \left(\dot{E}_{steam} - \dot{E}_{condensate}\right) + \dot{W}_{CC} - \dot{E}_{wCO_2} \quad (42)$$

where $\dot{I}_{CC}$ is the exergy destroyed due to irreversibilities, $\dot{E}_{water}$ is the exergy flow rate of the water removed in the separation process prior to the absorber, $\dot{E}_{g,inlet} - \dot{E}_{g,outlet}$ is the variation in exergy between the gases coming from the boiler and those treated by the system, $\left(\dot{E}_{MEA} + \dot{E}_{water}\right)_{makeup}$ is the exergy flow rate of the MEA and fill water supplied to the system, $\dot{E}_{WG,inlets} - \dot{E}_{WG,outlets}$ is the exergy variation between the water-glycol inlet and outlet flow rates, $\dot{W}_{CC}$ is the power supplied to the system and $\dot{E}_{wCO_2}$ is the exergy flow rate of the captured wet CO_2.

Some of the terms of the above equation can be grouped as follows:

$$\Delta\dot{E}_g = -\left(\dot{E}_{g,inlet} - \dot{E}_{g,outlet}\right) \quad (43)$$

$$\dot{E}_{makeup} = \left(\dot{E}_{MEA} + \dot{E}_{water}\right)_{makeup} \quad (44)$$

$$\Delta\dot{E}_{WG} = -\left(\dot{E}_{WG,inlets} - \dot{E}_{WG,outlets}\right) \quad (45)$$

$$\Delta\dot{E}_{steam} = -\left(\dot{E}_{steam} - \dot{E}_{condensate}\right) \quad (46)$$

$$\dot{E}_{dest} = \dot{I}_{CC} + \dot{E}_{water} \quad (47)$$

where $\dot{E}_{dest}$ includes the exergy destroyed by system irreversibilities and the residual exergy flow rate of the water removed in the separation process.

Substituting Eqs. (43), (44), (45), (46) y (47) in Eq. (42) yields:

$$\dot{E}_{dest} + \dot{E}_{wCO_2} = \dot{W}_{CC} + \dot{E}_{makeup} - \Delta\dot{E}_g - \Delta\dot{E}_{WG} - \Delta\dot{E}_{steam} \quad (48)$$

According to (48), the exergy efficiency of the CO_2 capture system ($\eta_{ex,CC}$) is defined as:

$$\eta_{ex,CC} = \frac{\dot{E}_{wCO_2}}{\dot{W}_{CC} + \dot{E}_{makeup} - \Delta\dot{E}_g - \Delta\dot{E}_{WG} - \Delta\dot{E}_{steam}} \quad (49)$$

3.7. Exergy efficiency of the FSRU

FSRU exergy balance during the regasification process is shown in Fig. 8.

Considering the decomposition of NG exergy into chemical exergy and the components of physical exergy, the exergy balance equation is:

$$\dot{I}_{FSRU} + \dot{E}_{g,outlet} + \dot{E}_{water} + \dot{E}_{non-cond} = \left[\left(\dot{E}^{p}_{LNG} + \dot{E}^{p}_{BOG}\right) - \left(\dot{E}^{p}_{NG} + \dot{E}^{p}_{cond}\right)\right] + \left[\left(\dot{E}^{th}_{LNG} + \dot{E}^{th}_{BOG}\right) - \left(\dot{E}^{th}_{NG} + \dot{E}^{th}_{cond}\right)\right] + \left[\left(\dot{E}^{ch}_{LNG} + \dot{E}^{ch}_{BOG}\right) - \left(\dot{E}^{ch}_{NG} + \dot{E}^{ch}_{cond}\right)\right] + \dot{E}_{air} + \dot{E}_{makeup} - \dot{E}_{LCO_2} \quad (50)$$

where $\dot{I}_{FSRU}$ is the exergy destroyed due to irreversibilities, $\dot{E}_{g,outlet}$ is the treated gas exergy flow rate, $\dot{E}_{water}$ is the exergy flow rate of the water removed in the separation processes, $\dot{E}_{non-cond}$ is the non-condensable gas exergy flow rate in the CO_2 liquefaction process, $\dot{E}_{air}$ is the exergy flow rate of the air required in the boiler combustion process, $\dot{E}_{makeup}$ is

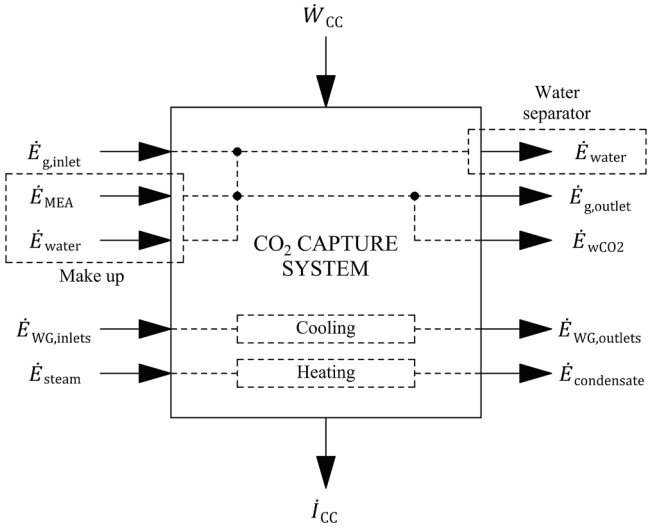

Fig. 7. Exergy balance of the CO_2 capture system.

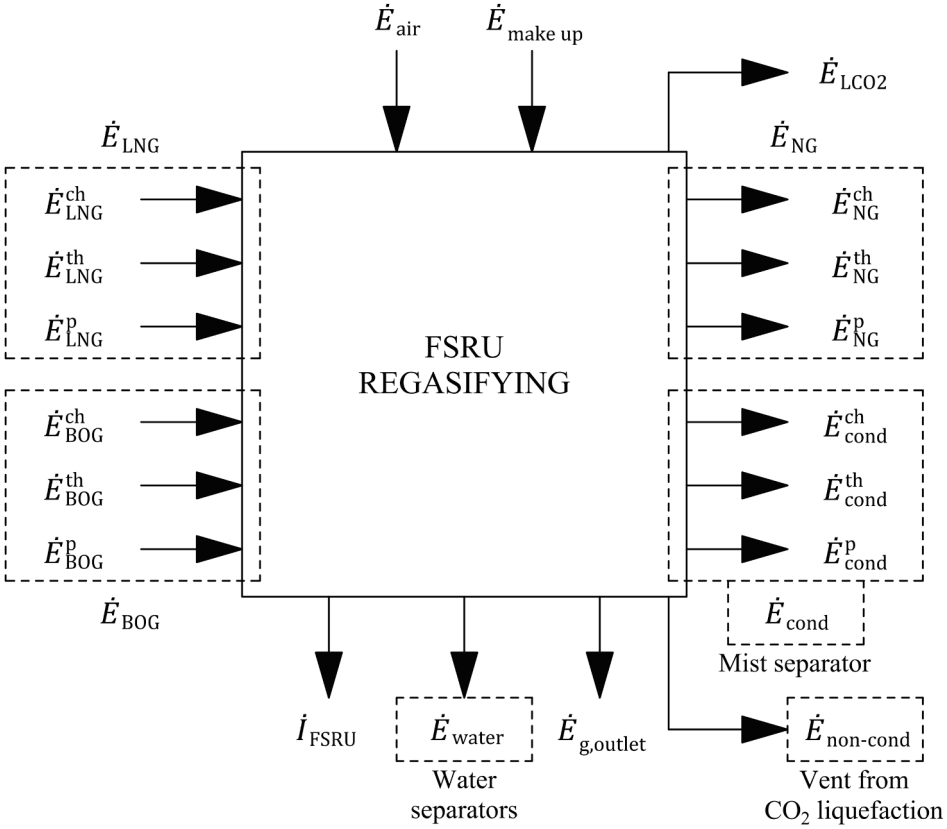

Fig. 8. Exergy balance of the FSRU.

the exergy flow rate of the MEA and fill water supplied to the system and $\dot{E}_{LCO_2}$ is the liquefied CO_2 exergy flow rate. Subscripts LNG and BOG of the equation represent the exergy flow rates associated with LNG and BOG from the tank, while NG and cond are the exergy flow rates of the regasified NG and the condensables collected by the mist separator. Condensable exergy flow rates are disregarded in the paper since the mass flow rate is either negligible (real NG composition) or nil (pure methane).

Some terms of the above equation can be replaced considering the following relationships:

$$\Delta\dot{E}^{p}_{NG} = -\left[\left(\dot{E}^{p}_{LNG}+\dot{E}^{p}_{BOG}\right)-\left(\dot{E}^{p}_{NG}+\dot{E}^{p}_{cond}\right)\right] \tag{51}$$

$$\Delta\dot{E}^{th}_{NG} = -\left[\left(\dot{E}^{th}_{LNG}+\dot{E}^{th}_{BOG}\right)-\left(\dot{E}^{th}_{NG}+\dot{E}^{th}_{cond}\right)\right] \tag{52}$$

$$\Delta\dot{E}^{ch}_{NG} = -\left[\left(\dot{E}^{ch}_{LNG}+\dot{E}^{ch}_{BOG}\right)-\left(\dot{E}^{ch}_{NG}+\dot{E}^{ch}_{cond}\right)\right] \tag{53}$$

$$\dot{E}_{dest} = \dot{I}_{FSRU}+\dot{E}_{g,outlet}+\dot{E}_{water}+\dot{E}_{non-cond} \tag{54}$$

where $\dot{E}_{dest}$ includes the exergy destroyed by the irreversibilities and the non-usable exergy flow rates that evolve to dead state conditions, such as those connected with the treated flue gases, the water removed by the separation processes and the liquefaction process non-condensable gases.

Replacing Eqs. (51), (52), (53) and (54) in Eq. (50) yields:

$$\dot{E}_{dest}+\Delta\dot{E}^{p}_{NG}+\dot{E}_{LCO_2} = \dot{E}_{air}+\dot{E}_{makeup}-\Delta\dot{E}^{ch}_{NG}-\Delta\dot{E}^{th}_{NG} \tag{55}$$

Based on Eq. (55), FSRU exergy efficiency ($\eta_{ex,FSRU}$) is defined as:

$$\eta_{ex,FSRU} = \frac{\Delta\dot{E}^{p}_{NG}+\dot{E}_{LCO_2}}{\dot{E}_{air}+\dot{E}_{makeup}-\Delta\dot{E}^{ch}_{NG}-\Delta\dot{E}^{th}_{NG}} \tag{56}$$

3.8. Environmental analysis

The environmental analysis is conducted assessing the CO_2 emissions generated by the FSRU during the regasification process. Two indices are used: the first -the Energy Efficiency Regasification Indicator (EERI)- focuses on CO_2 emissions resulting from fuel consumption, while the second -Carbon Footprint Regasification Indicator (CFRI)- determines equivalent CO_2 emissions and includes the beneficial effect of the CO_2 capture system.

The general equation of EERI is defined as [34]:

$$EERI = \frac{\sum_j \dot{m}_j C_{Fj}}{\dot{m}_{NG}(h_{NG}-h_{LNG})} \tag{57}$$

where $\dot{m}_j$ is the fuel mass flow rate, C_{Fj} is the non-dimensional conversion factor between fuel consumption and CO_2 emissions (g CO_2/g fuel), h_{NG} is the specific enthalpy of the regasified NG and h_{LNG} is the specific enthalpy of saturated liquid at the temperature of the LNG contained in the storage tanks with the same composition as the regasified NG.

Similar to the EERI, the general equation of CFRI is [34]:

$$CFRI = \frac{\sum_j \dot{m}_j C_{Fj}+\dot{m}_{CH_4}\left(GWP_{CH_4}-C_{F,CH_4}\right)-\dot{m}_{CC,RB}-\dot{m}_{CC,AE}}{\dot{m}_{NG}(h_{NG}-h_{LNG})} \tag{58}$$

where $\dot{m}_{CH_4}$ is the mass flow rate of methane in auxiliary engine exhaust gases, GWP_{CH_4} is the global warming potential (GWP) of methane, C_{F,CH_4} is the non-dimensional conversion factor between methane and CO_2 emissions and $\dot{m}_{CCS,RB}$ and $\dot{m}_{CCS,AE}$ are CO_2 mass flow rates captured by the carbon capture systems of regasification boilers and auxiliary engines, respectively.

Table 13
Input values for ORC validation from Yao et al. [20].

Parameter	Value
Mole fraction of methane in LNG	0.95
Mole fraction of ethane in LNG	0.30
Mole fraction of propane in LNG	0.20
LNG inlet temperature	−162 °C
LNG inlet pressure	5 bar
NG outlet temperature	5 °C
NG outlet pressure	80 bar
Water inlet temperature	20 °C
Water inlet pressure	1.5 bar
Water outlet temperature	15 °C
Subcooling degree of propane	2 °C
Minimum temperature difference	5 °C
Isentropic efficiency of the turbine	80%
Isentropic efficiency of the pumps	75%

Table 14
Comparison of the ORC results obtained in this study and by Yao et al. [20].

Parameter	Ref. [20]	This study	Absolute difference (–)	Percent difference (%)
Net power (kJ/kg)	28.69	27.39	1.30	4.54
Irreversibility (kJ/kg)	331.89	336.59	4.69	1.41

Table 15
Input values for the steam and condensate system validation from previous work [42].

Parameter	Value
BOG temperature	29.80 °C
BOG pressure	1.06325 bar
DSH-1 steam flow rate	0 kg/s
Steam mass flow rate for regasification process	30.75 kg/s

Table 16
Comparison of the steam and condensate system results obtained in this study and previous work [42].

Parameter	Ref. [42]	This study	Absolute difference (–)	Percent difference (%)
BOG consumption (kg/s)	1.90	1.90	0.00	0.00
Air flow rate (kg/s)	35.87	35.87	0.00	0.00
Boiler useful heat (kW)	84 832.89	84 827.67	5.22	0.01
Flue gas temperature (°C)	185.88	183.93	1.95	1.05

Considering that the ORC is designed to fulfil the FSRU's power demand, Eq. (58) can be simplified as:

$$CFRI = \frac{\sum_j \dot{m}_j C_{Fj} - \dot{m}_{CC,RB}}{\dot{m}_{NG}(h_{NG} - h_{LNG})} \quad (59)$$

3.9. Validation

Although the regasification system model developed in Aspen HYSYS v10 cannot be fully validated experimentally or through scientific literature, some subsystems can be simulated using input parameters from published papers, thus basing validation on the comparison of the results obtained.

The ORC architecture is identical to that studied in several papers on the exploitation of cold energy in FSRUs. Therefore, the ORC is simulated by introducing the input parameters corresponding to Table 13, which are those adopted by Yao et al. [20]. Table 14 shows that the net power developed by the ORC and the exergy destroyed by the irreversibilities differ by 4.54 and 1.41%, respectively.

With reference to the steam and condensate system, this was modelled in our previous work [42] using the EES. Adopting the simulation conditions of Table 15 yields almost identical results in the Aspen HYSYS, as shown in Table 16.

The CO_2 capture system is undoubtedly the most difficult to verify due to the number of input parameters required and because of the simulation methods. No previous studies have been found that address CO_2 capture in marine boilers although there are, however, studies related to CO_2 capture in propulsion systems on board. An attempt has been made to find a reference capture system most comparable to the one designed and proposed in this work for validation of the latter. The selected paper is to that of Luo et al. [13], who perform an experimental validation of a CO_2 capture system with MEA, developed in Aspen Plus for subsequent scaling to the flow rate of gases to be treated from the engines and gas turbine. The input parameters used for validation of the system are listed in Table 17. Since the only CO_2 content known is that of the gases at the absorber inlet, the composition of the boiler flue gases is normalised to reach the CO_2 content required in the simulation. Table 18 shows that the acid gas loading of lean amine solution renders the maximum percentage difference with a value of 8.77%, while the values of captured CO_2 and the specific reboiler duty are of 0.63 and 3.38%,

Table 17
Input values for the CO_2 capture system validation from Luo et al. [13].

Parameter	Value
Flue gas flow rate (kg/s)	40.13
Flue gas CO_2 content (mol%)	5.66
Solvent MEA content (wt%)	35
CO_2 capture efficiency (%)	90.00
L/G ratio (kg/kg)	2.06
Absorber diameter (m)	4.9
Absorber and stripper packing type	Mellapak 250Y
Absorber packing height (m)	12.5
Stripper diameter (m)	2.1
Stripper packing height (m)	6.5

Table 18
Comparison of the CO_2 capture system results obtained in this study and by Luo et al. [13].

Parameter	Ref. [13]	This study	Absolute difference (–)	Percent difference (%)
CO_2 captured (kg/s)	3.17	3.19	0.02	0.63
Lean loading (mol CO_2/mol MEA)	0.308	0.335	0.027	8.77
Rich loading (mol CO_2/mol MEA)	0.457	0.488	0.031	6.78
Reboiler duty (MW)	12.21	12.65	0.44	3.60
Specific reboiler duty (MJ/kg CO_2)	3.85	3.98	0.13	3.38

Table 19
Target variables of the simulation with their corresponding tolerance and adjusted variable.

Target variable	Value ± Tolerance	Adjusted variable
NG regasification temperature (T_8)	10.00 ± 0.01 °C	Forced BOG mass flow rate ($\dot{m}_{11}$)
Turbine electric power	Electric power demand ± 0.025 kW	Propane boiling point (T_{29})
Reboiler temperature (T_{84})	119.975 ± 0.025 °C	Steam mass flow rate ($\dot{m}_{42}$)
Steam temperature after DSH-1 (T_{49})	140.000 ± 0.001 °C	Water mass flow rate ($\dot{m}_{33}$)

Table 20
Main thermodynamic and environmental results.

Parameter	Value
BOG boiler consumption (kg/h)	6720.13
Specific energy consumption (kJ/kg)	831.03
Electric power demand (kW)	8774.63
Exergy supplied (kW)	214 442.73
Exergy destruction (kW)	140 518.70
FSRU exergy efficiency (%)	34.47
Regasification energy flow rate (kW)	85 088.48
EERI (g CO_2/MJ)	60.33
CFRI (g CO_2e/MJ)	6.16
CO_2 capture efficiency (%)	90.02
LCO_2 flow rate (kg/s)	4.61
LCO_2 purity (mol%)	99.967

Table 21
Results of the carbon capture system.

Parameter	Value
Flue gas flow rate (kg/s)	34.40
Flue gas CO_2 content (mol%)	9.78
Solvent MEA content (wt%)	30
L/G ratio (kg/kg)	3.40
Lean loading (mol CO_2/mol MEA)	0.261
Rich loading (mol CO_2/mol MEA)	0.444
Reboiler duty (kW)	21 616.25
Specific reboiler duty (kJ/kg CO_2)	4689.81
Absorber and stripper packing type	Mellapak 250Y
Absorber diameter (m)	4.417
Absorber packing height (m)	7.000
Stripper diameter stage 1–4/stage 5–10 (m)	1.317/2.633
Stripper packing height stage 1–4/stage 5–10 (m)	2.000/3.000

respectively. Considering that the present work focuses on the CO_2 capture capacity and the energy needs of this system, the results obtained from the comparison are deemed satisfactory.

4. Results and discussion

The complexity of the regasification system requires the application of the iterative method with the appropriate tolerances to facilitate the convergence of the simulation. This is performed in the Aspen HYSYS with a first approximate calculation in which the value of the manipulated variables is entered. The program then automatically iterates through the Adjuster blocks until the required tolerances of the target variables have been reached. Table 19 depicts the target variables with the corresponding tolerances and manipulated variables applied in the regasification system simulation.

Given the conditions and parameters assumed from section 3, and the mentioned tolerances, the lean amine solution flow rate capable of satisfying all the imposed requirements must be determined. Therefore, the required mass flow rate is obtained by increasing its value with a step size of 1 kg/s until a capture efficiency of at least 90.00% has been achieved. The simulations carried out suggest that the lean solution mass flow rate must be 117 kg/s to achieve a capture efficiency of 90.02%. Supplementary Table 1 provides the thermodynamic properties of each regasification system state, while Supplementary Table 2 comprises the compositions of the fluids and the chemical exergies necessary

Table 22
Power balance of the regasification system.

Equipment	Power (kW)	$\eta_{el,m}$ (%)	Electric power (kW)	Electric power weight (%)
FSRU auxiliary equipment	–	–	2050.90	23.37
C-1	289.56	90.00	321.73	3.67
C-2	285.42	90.00	317.13	3.61
FDF	183.09	90.00	203.44	2.32
FGB	187.42	90.00	208.24	2.37
LD	535.93	80.00	669.91	7.63
P-1	258.72	90.00	287.47	3.28
P-2	3452.86	90.00	3836.51	43.72
P-3	465.82	90.00	517.58	5.90
P-4	135.96	90.00	151.06	1.72
P-5	120.62	90.00	134.02	1.53
P-6	40.27	90.00	44.74	0.51
P-7	28.69	90.00	31.88	0.36
T	9236.47	95.00	8774.65	100.00

Table 23
Exergy destruction and exergy efficiency by equipment of the regasification system. (1) The output exergy is considered as an absolute value; however, the heat exchanger acts as a dissipative component. (2) Boiler system includes valves V-2 and V-5. (3) CCS includes all components of Fig. 3, except for the desuperheater system. (4) Desuperheater system includes valves V-6 and V-7. (5) FT system includes steam trap T-1. (6) ORC includes all components associated with the working fluid and valves V-3 and V-4. (7) PH system includes steam trap T-2.

Equipment	Input exergy (kW)	Output exergy (kW)	Irreversibilities (kW)	Exergy efficiency (%)
AC/NGH	4.84	2.16	7.00	44.59 (1)
Boiler	92 339.65	33 050.57	59 289.07	35.79
Boiler system (2)	92 831.06	30 750.29	62 080.77	33.13
C-1	289.56	239.01	50.55	82.54
C-2	285.42	235.68	49.74	82.57
CCS (3)	11343.32	2259.35	9166.92	19.92
DC	854.07	203.29	650.79	23.80
DSH-1	203.78	182.53	21.25	89.57
DSH-1 system (4)	1423.91	181.91	1242.00	12.78
FDF	183.09	147.04	36.06	80.31
FGB	187.42	152.26	35.16	81.24
FT	1804.21	552.96	1251.26	30.65
FT system (5)	1866.44	552.96	1313.49	29.63
LCO2	873.61	566.07	307.54	64.80
LD	535.93	259.93	276.00	48.50
MX	45.31	25.84	19.47	57.02
ORC (6)	58 934.72	8772.63	50 162.08	14.89
P-1	258.72	59.26	199.46	22.91
P-2	3452.86	842.20	2610.66	24.39
P-3	465.82	319.51	146.31	68.59
P-4	135.96	113.59	22.36	83.55
P-5	120.62	100.71	19.91	83.49
P-6	40.27	24.87	15.40	61.76
P-7	28.69	21.72	6.98	75.68
PH	2357.95	1592.61	765.34	67.54
PH system (7)	2439.28	1592.61	846.67	65.29
PVP	20 236.03	1773.78	18 462.25	8.77
R	0.00	0.00	0.00	–
RMH	4105.61	3198.01	907.60	77.89
T	12 012.78	9236.47	2776.31	76.89
T-1	62.23	0.00	62.23	–
T-2	81.33	0.00	81.33	–
T-3	66.90	0.00	66.90	–
V-1	214.17	0.00	214.17	–
V-2	0.00	0.00	0.00	–
V-3	327.81	0.00	327.81	–
V-4	3.15	0.00	3.15	–
V-5	2300.28	0.00	2300.28	–
V-6	0.62	0.00	0.62	–
V-7	1220.13	0.00	1220.13	–
V-8	491.42	0.00	491.42	–
V-9	16.54	0.00	16.54	–
V-10	17.02	0.00	17.02	–
VP	38 367.73	9919.48	28 448.24	25.85
WGC	7231.17	2160.05	5071.12	29.87
WGH-1	1968.14	911.15	2879.28	46.30 (1)
WGH-2	1120.03	850.60	1970.63	75.94 (1)
WGH-3	73.74	22.91	96.66	31.07 (1)
WGH-4	50.04	22.71	72.75	45.38 (1)
WGH-5	29.91	22.85	52.76	76.40 (1)

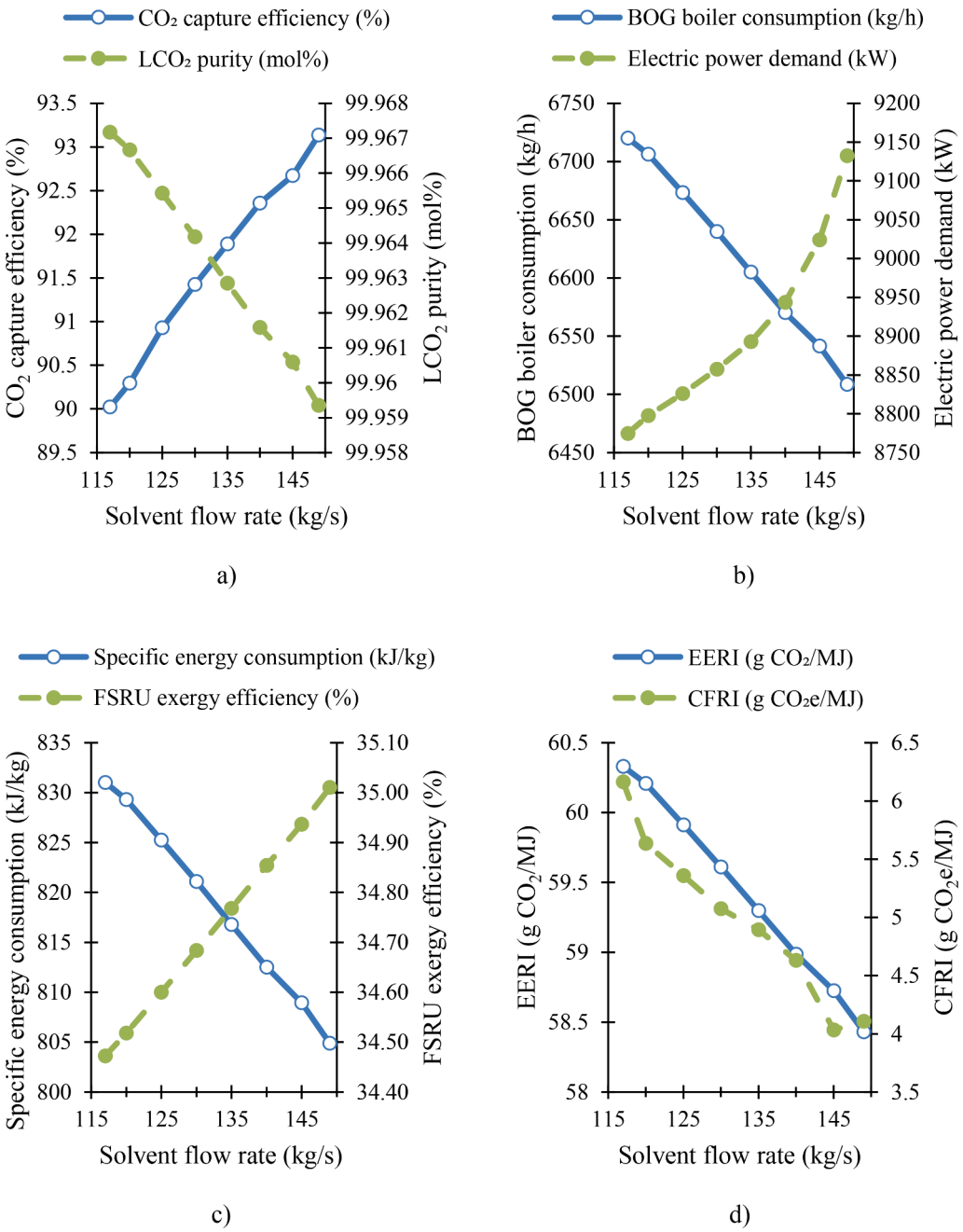

Fig. 9. Effect of increasing solvent flow rate: a) CO_2 capture efficiency and LCO_2 purity, b) BOG boiler consumption and electric power demand, c) specific energy consumption and FSRU exergy efficiency, d) EERI and CFRI.

for the exergy analysis. The main thermodynamic and environmental results of the regasification system are presented in Table 20, while Table 21 shows the results of the CO_2 capture process and column dimensions. The power consumed by each component, as well as the power produced by the ORC turbine, is given in Table 22. It is clear herein that the booster pump is the component of greatest power consumption and accounts for 43.72% of the electrical power demanded. Lastly, the exergy destroyed and the exergy efficiency of each relevant component and subsystem of the regasification system are presented in Table 23. The main exergy losses are due to the steam generation process in the boiler and the ORC methane and propane vaporizers.

The effect of key parameters such as lean solution flow rate, LNG composition, and LCO_2 purity are given below. Lastly, the proposed regasification system is compared, from a thermodynamic and environmental standpoint, with systems assessed in previous works.

4.1. *Effect of solvent flow rate*

Fig. 9 illustrates the effect caused by the variation of the solvent flow rate on the most relevant parameters of the regasification system. Capture efficiency undergoes an almost linear increase as the solvent flow rate increases until reaching 93.14% with a mass flow rate of 149 kg/s, although LCO_2 purity decreases slightly (see Fig. 9a). This solvent flow rate is the maximum possible value, since a higher value would prevent the ORC from being able to fully meet the FSRU's power demand, thus requiring the support of DF engines. Fig. 9b depicts the decrease in boiler fuel consumption and increase in power demand as the solvent flow rate approaches maximum value. At this limit, fuel consumption drops by 3.15% compared to that obtained for the minimum flow rate, while electric power demand increases by 4.08%. By keeping the lower calorific value of the BOG and the regasified NG mass flow rate constant,

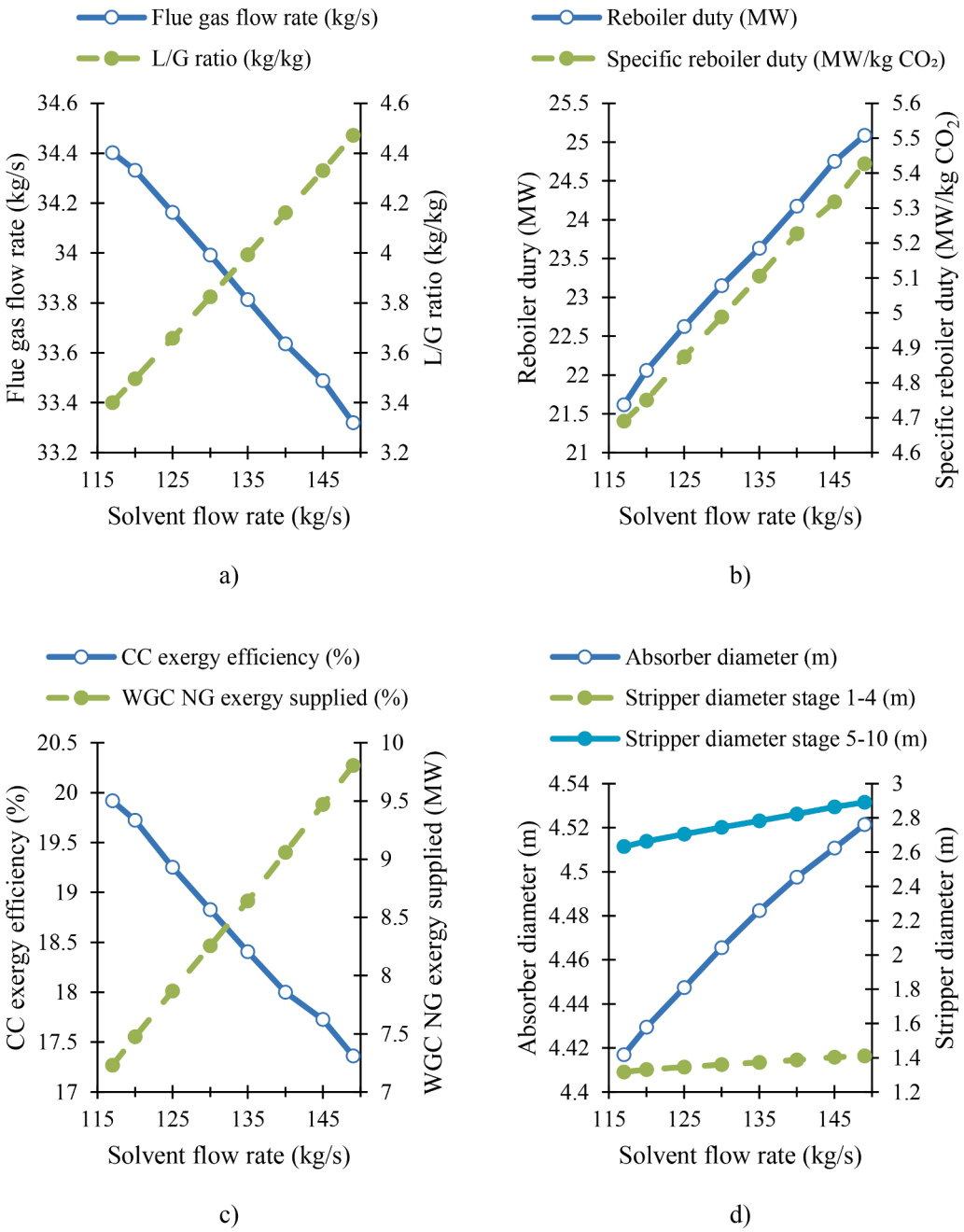

Fig. 10. Effect of increasing solvent flow rate on carbon capture system: a) flue gas flow rate and L/G ratio, b) reboiler duty and specific reboiler duty, c) exergy efficiency and LNG exergy supplied, d) absorber and stripper diameters.

specific energy consumption experiences the same decrease as fuel consumption (see Fig. 9c). This decrease implies an increase in FSRU exergy efficiency of 1.56%. Fig. 9d shows the decrease in EERI and CFRI with increasing solvent flow rate. In this case, regasification energy remains constant as neither the regasification flow rate nor the LNG composition varies. Therefore, the EERI is solely influenced by boiler fuel consumption, experiencing the same decrease as the specific energy consumption, while the drop in the CFRI is also susceptible to the flow rate of captured CO_2. Thus, the CFRI exhibits a less regular behaviour on the graph as it depends significantly on the calculations made by Aspen HYSYS of the columns of the CO_2 capture system and the tolerances allowed in the simulation. With maximum solvent flow rate, the CFRI decreases in value with respect to the minimum flow rate by 33.35%. To deeper assess the behaviour of the regasification system, the following paragraphs interpret the results of Figs. 10 and 11, which respectively present the relevant results of two subsystems: the CO_2 capture system and the ORC.

The increase in solvent flow rate causes a rise in L/G ratio in the absorber, which is incremented by the decrease in flow rate of gases to be treated (see Fig. 10a). With regard to the regeneration process, Fig. 10b illustrates that the increase in flow rate raises the duty in the reboiler, that is, a greater flow rate of steam from the desuperheater, while worsening the process efficiency due to the increase in specific duty. Another consequence of increasing solvent flow rate is greater cooling demand in the CO_2 capture system, causing a higher flow rate of water-glycol. As a result, the exergy efficiency of the CO_2 capture system drops by 12.83% with the maximum solvent flow rate, while the exergy supplied by the NG to the water-glycol cooler increases by 35.59% (see Fig. 10c). Regarding CO_2 capture system dimensioning, Fig. 10d displays the increase in the diameters of the absorption and regeneration

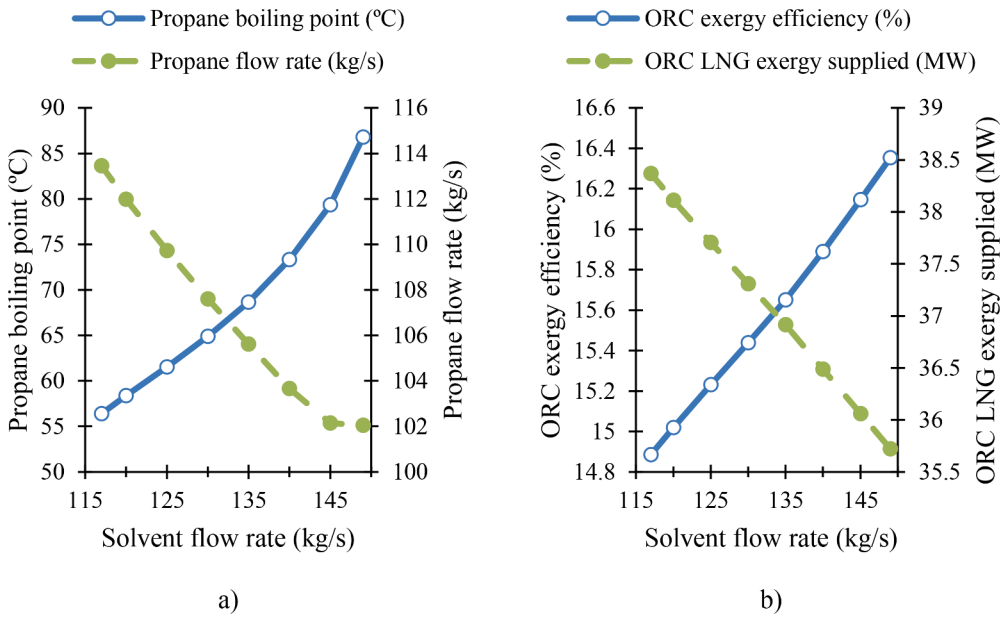

Fig. 11. Effect of increasing solvent flow rate on ORC: a) propane boiling point and flow rate, b) exergy efficiency and LNG exergy supplied.

columns as the solvent flow rate approaches maximum value.

Fig. 11a depicts how the propane boiling point increases as solvent flow rate increases, while the propane mass flow rate decreases. Increasing the boiling point brings about a greater enthalpy drop in the turbine, but also increases the specific power consumption in the propane pump since pressure in the vaporization process increases. Although the propane flow rate drops, the increase in pump power is significant enough to, in turn, increase the FSRU's power demand, as per Fig. 9b. This means that the enthalpy drop in the turbine can offset the drop in propane flow rate and increase the electrical power generated, thereby satisfying demand. The reason for the decrease in propane flow rate is a result of maintaining the NG regasification temperature at 10 °C as the solvent flow rate increases. This requirement causes the variation of energy flow rate and, by extension, that of exergy flow rate, to remain constant between the states corresponding to the booster pump discharge and NG output from the water-glycol cooler. Therefore, since the exergy supplied in the water-glycol cooler increases with solvent flow rate (see Fig. 10c), the exergy provided in the vaporizer must decrease by reducing propane flow rate. This can be seen in Fig. 11b, which shows the decrease in exergy flow rate provided in the NG vaporizer, and the increase in ORC exergy efficiency as the solvent flow rate increases. Decreasing the propane flow rate reduces the steam demand in the propane vaporizer to such an extent that the overall steam demand is affected, causing the boiler fuel consumption to drop, as seen above in Fig. 9b.

Table 24
Main results of the effect of LNG composition.

Parameter	Value	Difference (–)	Percent difference (%)
Process performance			
BOG boiler consumption (kg/h)	6284.16	−435.96	−6.49
Specific energy consumption (kJ/kg)	781.27	−49.75	−5.99
Electric power demand (kW)	8413.37	−361.26	−4.12
Exergy supplied (kW)	193 369.54	−21 073.20	−9.83
Exergy destruction (kW)	128 512.97	−12 005.72	−8.54
FSRU exergy efficiency (%)	33.54	−0.93	−2.70
Regasification energy flow rate (kW)	80 205.29	−4883.19	−5.74
EERI (g CO_2/MJ)	59.85	−0.48	−0.79
CFRI (g CO_2e/MJ)	5.22	−0.94	−15.26
CO_2 capture efficiency (%)	90.73	0.71	0.79
LCO_2 flow rate (kg/s)	4.38	−0.23	−4.93
LCO_2 purity (mol%)	99.966	−0.001	0.00
CO_2 capture system			
Flue gas flow rate (kg/s)	32.01	−2.39	−6.95
Flue gas CO_2 content (mol%)	9.87	0.08	0.84
L/G ratio (kg/kg)	3.65	0.25	7.47
Lean loading (mol CO_2/mol MEA)	0.262	0.00	0.15
Rich loading (mol CO_2/mol MEA)	0.434	−0.01	−2.17
Reboiler duty (kW)	21 203.90	−412.35	−1.91
Specific reboiler duty (kJ/kg CO_2)	4839.17	149.36	3.18
Absorber diameter (m)	4.305	−0.112	−2.53
Stripper diameter stage 1–4 (m)	1.303	−0.014	−1.04
Stripper diameter stage 5–10 (m)	2.618	−0.015	−0.56

4.2. *Effect of LNG composition*

Table 24 presents the main results of the regasification system if the composition of the LNG stored in the tank is that of Table 2. When the composition is with pure methane, boiler fuel consumption drops by 6.49%, while specific energy consumption decreases by 5.99%. This is due to the fact that, with the mentioned composition, LNG is -from a thermodynamic standpoint- easier to regasify than pure methane, as can be seen in the decrease in regasification energy flow rate of 5.74%. Particular attention, therefore, must be given to the NG temperature at the CO_2 liquefier inlet.

Although the FSRU's electrical power demand drops by 4.12%, propane boiling temperature increases to offset the decrease in steam flow rate in the propane vaporizer and increase the enthalpy drop in the turbine. As a result, the propane mass flow rate decreases and, consequently, the heat flow rate exchanged between the LNG and propane lessens, yet this is not enough to prevent the NG temperature at the ORC outlet from increasing. Moreover, the CO_2 liquefaction temperature at a pressure of 6.5 bar is below that of the NG at the liquefier inlet and, therefore, CO_2 pressure in the two compression stages must be increased from 7.5 to 9.9 bar so that the minimum temperature difference in the liquefier is kept above 5 °C. Lastly, CO_2 liquefaction temperature is −42.97 °C; this being an increase of 8.11 °C when compared with the case of pure methane. On the basis of this explanation and considering

the effect of solvent flow rate, it follows that increasing the flow rate of the lean solution can reduce the liquefaction pressure, since the heat flow rate exchanged between propane and LNG is less. For example, if the system is simulated with a solvent flow rate of 120 kg/s, the compression process pressure drops to 9.6 bar.

Moreover, the positive effect of a lower fuel consumption does not imply that the system is more efficient from an exergy viewpoint. Despite the decrease in exergy supplied and exergy destruction of the FSRU, exergy efficiency decreases by 2.70%.

The values of the EERI and CFRI decline 0.79 and 15.26%, respectively. Despite assessing CO_2 fuel consumption emissions, the EERI is, in fact, a better FSRU energy efficiency indicator than the specific energy consumption when comparing LNGs with different composition, since it is determined from the regasification energy flow rate and not just limited to the regasified NG mass flow rate. The percentage difference of the CFRI is significant when compared to the EERI. With the CFRI, fuel consumption reduction is doubly beneficial since, as well as reducing combustion CO_2 emissions, the flow rate of gases to be treated is reduced, thereby increasing the L/G ratio and, by extension, increasing capture efficiency. Furthermore, dimensioning of the CO_2 capture system is improved as the column diameters are slightly reduced.

Comparison of the LNG compositions determines that pure methane offers a more moderate and adequate position for most thermodynamic, environmental and dimensioning results when used as a reference composition. Care must be taken, however, when establishing the CO_2 liquefaction pressure.

4.3. *Effect of LCO_2 purity*

The main results of the increase in LCO_2 purity are set out in Fig. 12.

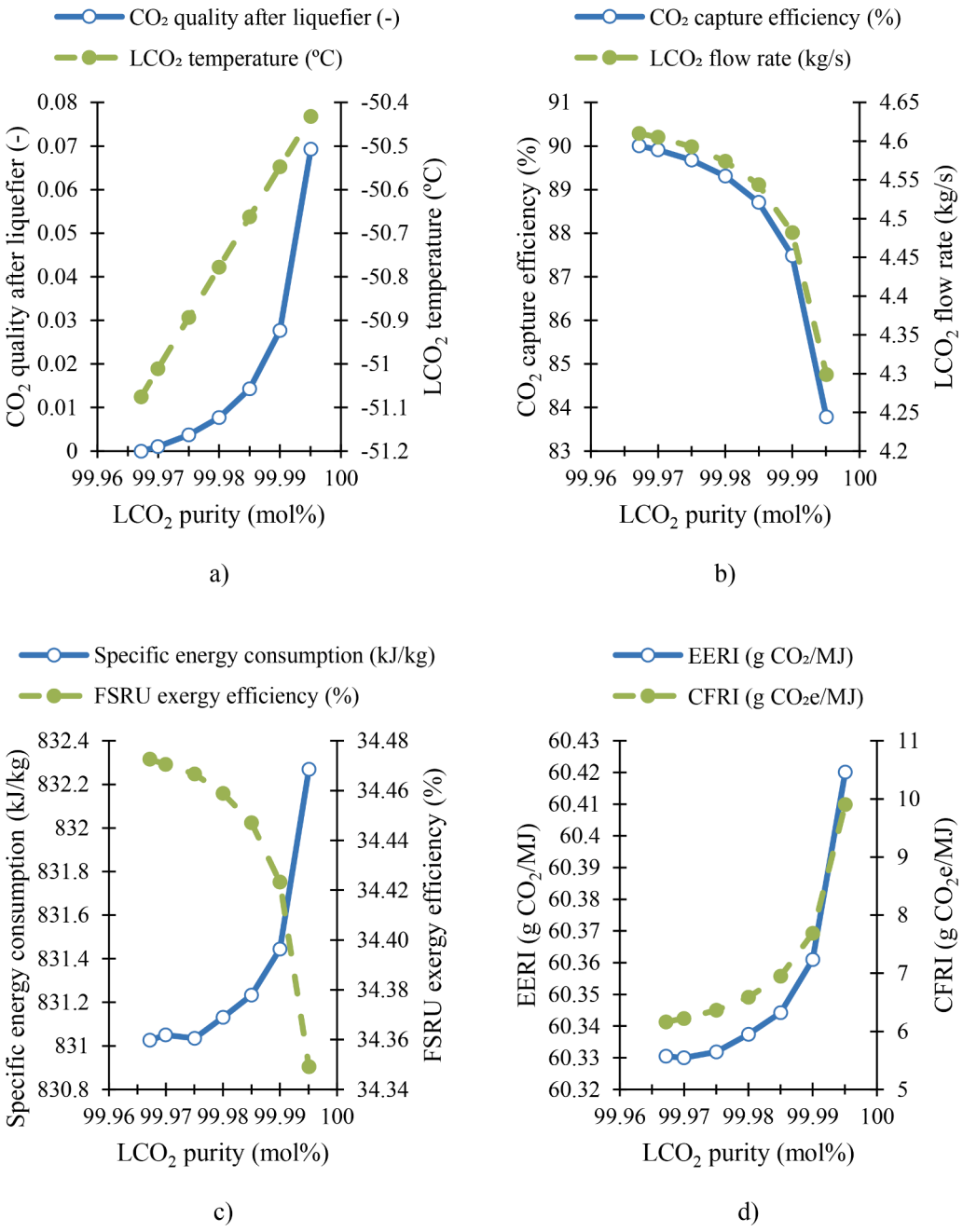

Fig. 12. Effect of increasing LCO_2 purity: a) CO_2 vapour quality after liquefier and LCO_2 temperature, b) CO_2 capture efficiency and LCO_2 flow rate, c) specific energy consumption and FSRU exergy efficiency, d) EERI and CFRI.

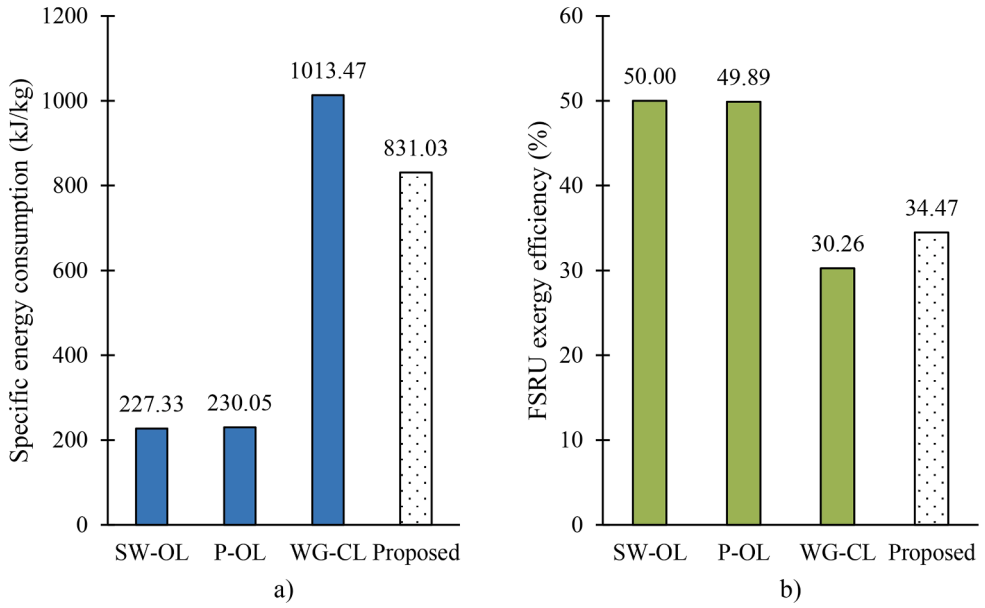

Fig. 13. Comparison of the proposed regasification system with regasification systems of previous work [42]: a) specific energy consumption, b) FSRU exergy efficiency.

As the vapour quality at the liquefier outlet increases, nitrogen content in the liquid phase drops and LCO_2 temperature rises approaching pure CO_2 saturation temperature (see Fig. 12a). Capture efficiency and LCO_2 flow rate drop sharply, however, with increasing LCO_2 purity, particularly from a purity of 99.990% (see Fig. 12b). Furthermore, increasing the vapour quality reduces the heat flow rate transferred in the liquefier, favouring a slight rise in specific energy consumption; that is, boiler fuel consumption, which, together with the decrease in LCO_2 flow rate, slightly reduce the exergy efficiency of the FSRU, as per Fig. 12c. Fig. 12d demonstrates that the impact of the increase in purity is more significant on the CFRI than the EERI, since the EERI is affected solely by the slight increase in fuel consumption. Reduced LCO_2 flow rate means an increase in the CFRI of 60.61% for a 99.995% purity in comparison with total liquefaction of CO_2 flow rate.

4.4. Comparison with other regasification systems

The regasification system studied herein is thermodynamically compared in Fig. 13 with the main systems installed in FSRUs: seawater system (SW-OL), open-loop propane system (P-OL), and closed loop water-glycol system (WG-CL). Fig. 13a illustrates that the closed-loop system proposed reduces specific energy consumption by 18.00% compared with the conventional water-glycol system. Despite this significant decrease, the value is still 3.7 times greater than open-loop regasification systems. As for the exergy analysis, Fig. 13b demonstrates that the proposed system is 13.91% more efficient than the water-glycol system.

CO_2 emissions per regasification energy of the FSRU for the above systems are depicted in Fig. 14. Two regasification systems are further included: a seawater system without recondenser that burns excess BOG in the GCU (GCU-OL), and an open-loop propane system with a simple

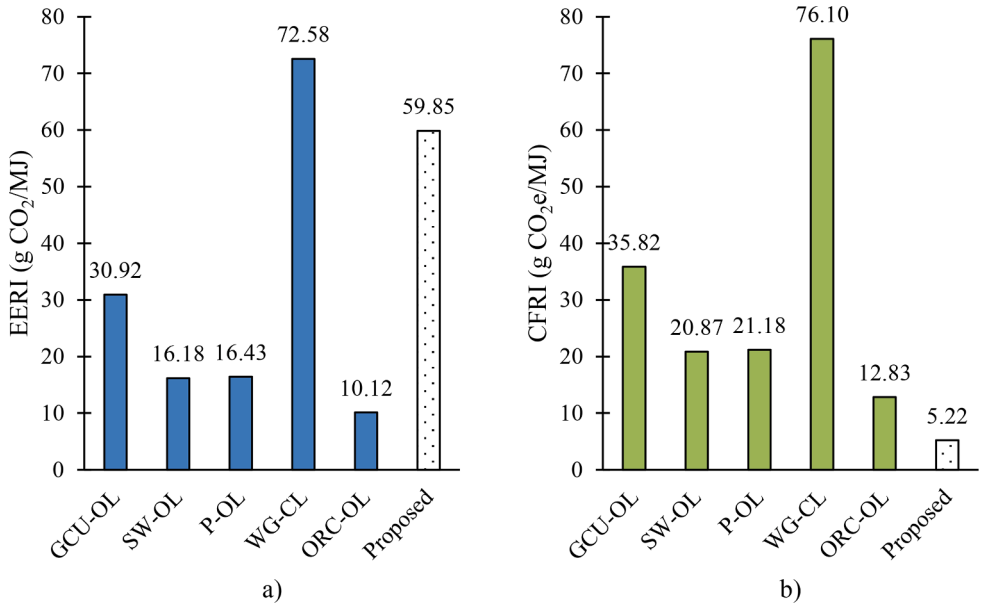

Fig. 14. Comparison of the proposed regasification system with regasification systems of previous work [34]: a) EERI, b) CFRI.

ORC (ORC-OL). In this case, to compare the proposed system with the other systems under the same simulation conditions, the results obtained with the LNG composition of Table 2 were used. If the open-loop system with lowest EERI is taken as a reference, that is, the open-loop system with ORC, the value obtained for the proposed system is 5.92 times greater (see Fig. 14a). Fig. 14b, however, indicates that the closed-loop system with CO_2 capture reduces the CFRI by 59.27% with respect to the same system, and does not produce methane emissions connected with the combustion process of DF engines. If the closed-loop water-glycol system is taken as reference, the EERI and CFRI of the proposed system are 17.54 and 93.14% lower, respectively.

In summary, the proposed regasification system is significantly more efficient than the conventional closed-loop system, despite consuming more energy than open-loop systems. This is owing to the fact that boiler fuel consumption is used for electrical energy production and CO_2 capture, achieving lower CO_2 emission levels than open-loop systems without making use of seawater during the regasification process.

5. Conclusions

A novel closed-loop regasification system for FSRUs that integrates an ORC for electrical power production and a chemical-absorption CO_2 capture system with MEA has been analysed in the present study from a thermodynamic and environmental standpoint. Captured CO_2 is liquefied using cold energy from the regasification process. The main conclusions drawn from the study are as follows:

- The regasification system designed for a CO_2 capture efficiency of 90.02% is capable of producing enough electrical power in the ORC to fully satisfy the demand of the FSRU. Under these conditions, the thermodynamic results obtained demonstrate that the specific energy consumption and exergy efficiency are of 831.03 kJ/kg and 34.47%, respectively. With regard to the environmental results, the EERI and CFRI obtained are respectively 60.33 g CO_2/MJ and 6.16 g CO_2e/MJ.
- The increase in solvent flow rate allows for a better capture efficiency, but there is a maximum value delimited by the capacity of the ORC to meet the FSRU's electrical power demand. As solvent flow rate increases, the cold energy/exergy required by the capture system also increases, reducing the contribution to the ORC. This results in a lower propane mass flow rate and an increase in boiling temperature to ensure that the turbine continues to meet the electrical power demand of the FSRU. Consequently, boiler fuel consumption decreases, as does the specific energy consumption, the EERI and the CFRI, while the exergy efficiency of the FSRU and the diameters of the absorber and regenerator columns increase.
- Analysis of the different LNG compositions shows that pure methane generally presents more moderate results than the composition in Table 2. Pure methane, therefore, is a suitable reference composition for system calculations. However, a compression pressure of the captured CO_2 must be set high enough to ensure that the liquefaction process can be performed with actual LNG compositions.
- LCO_2 purity can be improved by increasing the vapour quality at the liquefier outlet, with hardly any impact on specific energy consumption, exergy efficiency or the EERI. However, CO_2 capture efficiency and the CFRI are significantly affected as purity increases, particularly for values above 99.990%.
- The proposed regasification system is more efficient than the closed-loop water-glycol system installed in FSRUs: specific energy consumption drops 18.00%, while exergy efficiency increases 13.91%. Despite this significant improvement, fuel consumption remains high and, consequently, the results of the aforementioned parameters are rather far from those obtained for open-loop regasification systems. The proposed regasification system does, however, achieve CO_2 emissions four times under those of open-loop systems usually installed in FSRUs without making any use of seawater during the regasification process. Furthermore, when compared with an open-loop system that exploits cold energy through a simple ORC, the CFRI of the proposed system is 59.27% lower.

Carbon capture systems provide a potential solution to reduce CO_2 emissions from the maritime sector, including those vessels that are not used for transport, as is the case of FSRUs. The development of new closed-loop regasification systems that combine LNG cold energy exploitation with CO_2 capture is essential if a better efficiency is to be achieved and to drastically cut CO_2 emissions produced in the FSRU regasification process.

CRediT authorship contribution statement

Manuel Naveiro Parga: Writing – original draft, Conceptualization, Methodology, Visualization, Software, Writing – review & editing, Supervision. **Manuel Romero Gómez:** Conceptualization, Writing – review & editing, Supervision. **Ignacio Arias Fernández:** Writing – review & editing. **Álvaro Baaliña Insua:** Writing – review & editing.

Declaration of Competing Interest

The authors declare that they have no known competing financial interests or personal relationships that could have appeared to influence the work reported in this paper.

Acknowledgements

Funding for open access charge: Universidade da Coruña/CISUG.

Appendix A. Supplementary data

Supplementary data to this article can be found online at https://doi.org/10.1016/j.enconman.2022.115410.

References

[1] International Energy Agency. World Energy Outlook 2021. 2021.
[2] International Energy Agency. World Energy Outlook 2021 - Executive Summary. 2021.
[3] IMO. Fourth IMO GHG Study 2020 Executive Summary 2021.
[4] IMO. MEPC.304(72) Initial IMO Strategy on Reduction of GHG Emissions from Ships 2018.
[5] IMO. Further shipping GHG emission reduction measures adopted 2021. https://www.imo.org/en/MediaCentre/PressBriefings/pages/MEPC76.aspx (accessed November 6, 2021).
[6] Xing H, Stuart C, Spence S, Chen H. Alternative fuel options for low carbon maritime transportation: pathways to 2050. J Clean Prod 2021;297:126651. https://doi.org/10.1016/j.jclepro.2021.126651.
[7] Xing H, Spence S, Chen H. A comprehensive review on countermeasures for CO2 emissions from ships. Renew Sustain Energy Rev 2020;134:110222. https://doi.org/10.1016/j.rser.2020.110222.
[8] Alfa Laval. Alfa Laval and NMRI have succeeded in onboard CO2 capture testing using an exhaust gas cleaning system 2021. https://www.alfalaval.com/industries/marine-transportation/marine/marine-news/alfa-laval-and-nmri-have-succeeded-in-onboard-co2-capture-testing-using-an-exhaust-gas-cleaning-system/ (accessed November 10, 2021).
[9] Mitsubishi Heavy Industries. Mitsubishi Shipbuilding to Test World's First Marine-based CO2 Capture System – "CC-Ocean" Project in Partnership with "K" Line and ClassNK Part of Japan Government Initiative to Support Development of Marine Resource Technologies – 2020. https://www.mhi.com/news/20083101.html (accessed November 10, 2021).
[10] Wärtsilä. Wärtsilä advances carbon capture and storage in maritime as part of LINCCS consortium 2021. https://www.wartsila.com/media/news/08-09-2021-wartsila-advances-carbon-capture-and-storage-in-maritime-as-part-of-linccs-consortium-2972116 (accessed November 10, 2021).
[11] Mitsubishi Heavy Industries. Overview of "CC - Ocean" project 2021.
[12] Mitsubishi Heavy Industries. Mitsubishi Shipbuilding Begins Verification Testing of Marine-based CO2 Capture System 2021. https://www.mhi.com/news/21080501.html?style=preview (accessed November 3, 2021).
[13] Luo X, Wang M. Study of solvent-based carbon capture for cargo ships through process modelling and simulation. Appl Energy 2017;195:402–13. https://doi.org/10.1016/j.apenergy.2017.03.027.

[14] Feenstra M, Monteiro J, van den Akker JT, Abu-Zahra MRM, Gilling E, Goetheer E. Ship-based carbon capture onboard of diesel or LNG-fuelled ships. Int J Greenh Gas Control 2019;85:1–10. https://doi.org/10.1016/j.ijggc.2019.03.008.
[15] Lee S, Yoo S, Park H, Ahn J, Chang D. Novel methodology for EEDI calculation considering onboard carbon capture and storage system. Int J Greenh Gas Control 2021;105:103241. https://doi.org/10.1016/j.ijggc.2020.103241.
[16] Stec M, Tatarczuk A, Iluk T, Szul M. Reducing the energy efficiency design index for ships through a post-combustion carbon capture process. Int J Greenh Gas Control 2021;108:103333. https://doi.org/10.1016/j.ijggc.2021.103333.
[17] Long NVD, Lee DY, Kwag C, Lee YM, Lee SW, Hessel V, et al. Improvement of marine carbon capture onboard diesel fueled ships. Chem Eng Process - Process Intensif 2021;168:108535. https://doi.org/10.1016/j.cep.2021.108535.
[18] Ji C, Yuan S, Huffman M, El-Halwagi MM, Wang Q. Post-combustion carbon capture for tank to propeller via process modeling and simulation. J CO2 Util 2021;51:101655. https://doi.org/10.1016/j.jcou.2021.101655.
[19] Güler E, Ergin S. An investigation on the solvent based carbon capture and storage system by process modeling and comparisons with another carbon control methods for different ships. Int J Greenh Gas Control 2021;110:103438. https://doi.org/10.1016/j.ijggc.2021.103438.
[20] Yao S, Liu H, Tang L, Ye Y, Zhang L. Thermodynamic analysis and optimization for cold energy utilization based on low temperature rankine cycle of LNG-FSRU regasification system. Int J Simul Syst Sci Technol 2016. https://doi.org/10.5013/IJSSST.a.17.30.35. 17:35.1-35.9.
[21] Lee S, Choi BC. Thermodynamic assessment of integrated heat recovery system combining exhaust-gas heat and cold energy for LNG regasification process in FSRU vessel. J Mech Sci Technol 2016;30(3):1389–98. https://doi.org/10.1007/s12206-016-0246-y.
[22] Yoon-Ho L. LNG-FSRU cold energy recovery regasification using a zeotropic mixture of ethane and propane. Energy 2019;173:857–69. https://doi.org/10.1016/j.energy.2019.02.111.
[23] Yoon-Ho L. Thermo-economic analysis of a novel regasification system with liquefied-natural-gas cold-energy. Int J Refrig 2019;101:218–29. https://doi.org/10.1016/j.ijrefrig.2019.03.022.
[24] Yao S, Xu L, Tang L. New cold-level utilization scheme for cascade three-level Rankine cycle using the cold energy of liquefied natural gas. Therm Sci 2019;23(6 Part B):3865–75. https://doi.org/10.2298/TSCI171012239Y.
[25] Xu L, Lin G. Simulation and optimization of liquefied natural gas cold energy power generation system on floating storage and regasification unit. Therm Sci 2021;25(6 Part B):4707–19. https://doi.org/10.2298/TSCI200404205X.
[26] Mitsui O.S.K. Lines. MOL and DSME Obtain AIP for Design of FSRU "Cryo-Powered Regas" System - Development of New Technology to Reduce Environmental Impact - 2020.
[27] Songhurst B. Floating LNG update. Oxford, United Kingdom: 2019. doi:10.26889/9781784671440.
[28] U.S. Coast Guard; engineering-environmental Management. Neptune LNG Deepwater Port License Application: Environmental Impact Statement. 2006.
[29] Janssens P. The development of the first Energy Bridge regasification vessel. Offshore Technol Conf 2006 New Depths. New Horiz 2006;3:2052–63. https://doi.org/10.4043/18398-ms.
[30] Songhurst B. The Outlook for Floating Storage and Regasification Units (FSRUs). Oxford, United Kingdom: 2017. doi:10.26889/9781784670894.
[31] IMO. MEPC.308(73) 2018 Guidelines on the method of calculation of the attained Energy Efficiency Design Index (EEDI) for new ships 2018.
[32] Romero Gómez J, Romero Gómez M, Lopez Bernal J, Baaliña IA. Analysis and efficiency enhancement of a boil-off gas reliquefaction system with cascade cycle on board LNG carriers. Energy Convers Manag 2015;94:261–74. https://doi.org/10.1016/j.enconman.2015.01.074.
[33] Migliore C, Tubilleja C, Vesovic V. Weathering prediction model for stored liquefied natural gas (LNG). J Nat Gas Sci Eng 2015;26:570–80. https://doi.org/10.1016/j.jngse.2015.06.056.
[34] Naveiro M, Romero Gómez M, Arias Fernández I, Baaliña Insua Á. Energy efficiency and environmental measures for Floating Storage Regasification Units. J Nat Gas Sci Eng 2021;96:104271. https://doi.org/10.1016/j.jngse.2021.104271.
[35] Song Y, Chen C-C. Symmetric electrolyte nonrandom two-liquid activity coefficient model. Ind Eng Chem Res 2009;48(16):7788–97. https://doi.org/10.1021/ie9004578.
[36] Aspen Technology. Aspen HYSYS v10 2017.
[37] Dubois L, Thomas D. Comparison of various configurations of the absorption-regeneration process using different solvents for the post-combustion CO2 capture applied to cement plant flue gases. Int J Greenh Gas Control 2018;69:20–35. https://doi.org/10.1016/j.ijggc.2017.12.004.
[38] Frangopoulos CA. Exergy, Energy System Analysis and Optimization Volume - I: Exergy and Thermodynamic Analysis. Oxford, United Kingdom: EOLSS Publications; 2009.
[39] Szargut J. Exergy method: technical and ecological applications. WIT Press; 2005.
[40] Bejan A, Tsatsaronis G, Moran M. Thermal Design and Optimization. John Wiley & Sons, Ltd; 1996.
[41] Sato N. Chemical energy and exergy: an introduction to chemical thermodynamics for engineers. Elsevier 2004. https://doi.org/10.1016/B978-0-444-51645-9.X5000-6.
[42] Naveiro M, Romero Gómez M, Baaliña Insua Á, Folgueras MB. Energy, exergy and economic analysis of offshore regasification systems. Int J Energy Res 2021;45(15):20835–66. https://doi.org/10.1002/er.7141.